Journal of the Korean Ceramic Society (2022) 59:271–288
https://doi.org/10.1007/s43207-022-00198-w

REVIEW

Progress and perspectives of metal-ion-substituted hydroxyapatite for bone tissue engineering: comparison with hydroxyapatite

Si Hyun Kim[3] · Cheol Hyun Park[1] · Jun Hyuk Heo[1,2] · Jung Heon Lee[1,2,3,4]

Received: 21 December 2021 / Revised: 8 February 2022 / Accepted: 21 March 2022 / Published online: 2 May 2022

Abstract

Hydroxyapatite (HA) is one of the most common bioceramics and is abundant in human bones. HA is composed of calcium phosphate, which is prevalent in biomedical processes, particularly bone formation, osteogenesis, and angiogenesis. As HA is one of the core materials that makes up the human body, there has been considerable research on methods of synthesizing HA while changing its properties by substituting various types of metal ions. In particular, previous studies have intensively investigated the size, crystallinities, and morphologies generated using various synthesis methods to change the characteristics of HA by substituting different metal ions. This review summarizes the findings of these studies on HA, including findings on the characteristics of HA in natural bone, methods of synthesizing HA, and findings on metal-ion-substituted HA. Furthermore, the characteristics and applications of HA that were investigated in previous studies are summarized, and the latest trends and perspectives on the future of the field are also presented.

Keywords Hydroxyapatite (HA) · Metal ions · Substitution · Bone tissue engineering · Osteogenesis

1 Introduction

Hydroxyapatite (HA) is a type of bioceramic that has recently been used in several biological applications. In particular, as the ratio of calcium phosphate (CaP) is very similar to that of natural bone, HA is feasible for use in the treatment of bone defects [1]. In addition, HA has biomineralization properties similar to hard tissue; hence, it is currently used in orthopedics and dentistry [2–6]. HA is also used for other biomedical applications such as coating metallic osseous implants, drug delivery, and tissue engineering scaffolds because of its stoichiometric properties that are similar to bone, as well as other advantages such as biocompatibility, intimacy with other biopolymers, and excellence in inducing bone differentiation [7–13]. Over the past few decades, many researchers have attempted to synthesize the natural forms of HA.

Many studies have reported various synthesis methods for HA with different characteristics, such as size, morphology, stoichiometry, and crystallinity [14, 15]. In addition, many studies on the physicochemical properties of HA have been conducted for use in broad applications, including bone scaffolds, bone fillers, and implant coating applications [16–19].

Metal ion substitution into the HA structure has been attempted by many researchers to mimic the mineral composition of natural bone and enhance the properties of HA. Certain metal ions have been shown to increase the bioactivity and bone regeneration ability of HA. For example, strontium ions (Sr^{2+}), magnesium ions (Mg^{2+}), and zinc ions (Zn^{2+}) promote bone regeneration by acting as active regulators of osteoblasts and osteoclasts [20]. Therefore, over

Si Hyun Kim and Cheol Hyun Park have contributed equally to this work.

✉ Jun Hyuk Heo
saegusa@skku.edu

✉ Jung Heon Lee
jhlee7@skku.edu

1 School of Advanced Materials Science and Engineering, Sungkyunkwan University (SKKU), Suwon 16419, Republic of Korea

2 Advanced Materials Technology Research Center, Sungkyunkwan University (SKKU), Suwon 16419, Republic of Korea

3 SKKU Advanced Institute of Nanotechnology (SAINT), Sungkyunkwan University (SKKU), Suwon 16419, Republic of Korea

4 Biomedical Institute for Convergence at SKKU (BICS), Sungkyunkwan University (SKKU), Suwon 16419, Republic of Korea

several decades, researchers have investigated the development of methods for the synthesis of metal-substituted HAs. In this review, we mainly focus on the different synthesis methods of metal ion-substituted HA and highlight the properties exhibited when using different types of metal ions. To clearly explain the difference in the synthesis and properties of metal ion-substituted HA materials with bare HA, we will start from the discussion of bare HA.

2 Basic properties of HA

2.1 Chemical properties of HA

Calcium phosphate (CaP), which is the main constituent of natural human bone, accounts for 65% of the total bone mass. The remainder is composed of approximately 25% of collagen and other proteins, with less than 10% of water. In addition, the structure and chemical formula of CaP can vary depending on the Ca/P ratio (Table 1), which is influenced by whether it is in a natural or synthetic product and also leads to differences in biodegradation and bioresorption [21]. Biological apatite has a nanosized inorganic crystal structure, which forms an inorganic–organic nanocomposite with a collagen matrix and acts as a scaffold for deposition and crystal growth in bones [22]. Hydroxyapatite (HA), whose mineral composition is most similar to that of biological apatite in natural bones, is the most thermodynamically stable CaP source. However, studies have reported that actual biological apatites are calcium-deficient carbonates with Ca/P ratios of less than 1.67 [23–25].

It is well known that the pH value, along with calcium and phosphate ratios, is important when HA is implanted as bone scaffolds. For example, the pH value plays a role in determining the phase transformation of CaP [26]. It has been reported that the pH value can affect the dissolution rate of HA during calcium release [27]. Most importantly, as HA is exposed to the biological environment, abrupt pH variations can cause disintegration. As such, pH levels can potentially interfere with cell adhesion or angiogenesis and ultimately increase cytotoxicity, thus disrupting the regenerative process [28].

Bone must not only have sufficient strength but also be capable of hydrolysis and degradation processes under biological conditions [29]. However, HA typically shows the slowest degradation rate among crystalline forms of CaP. Its porosity, structure, and phase may affect the dissolution rate of HA [30]. In addition, the size and crystallinity of HA are crucial factors in determining its solubility. Generally, it is known that the low crystallinity and small size of HA can lead to high dissolubility under biological conditions. Recently, nano-HA has been attracting attention for use as scaffolds in bone tissue engineering because of its similar size and crystallinity to natural bone materials [23].

2.2 Physical properties of HA

Bones perform a range of mechanical functions in the human body, such as protecting vital organs and maintaining the structure of the body. They can also serve as axis during muscle movements. Collagen, the main organic component of bone, forms a nanocomposite with HA, which strengthens the intrinsically brittle mineral crystals, leading to bones with both strength and elasticity. HA can be characterized according to the particle's composition, crystallinity, crystallographic structure, growth orientation, shape, and size. The unit cell of HA has a hexagonal structure according to the lattice parameters ($a = 0.95$ nm, $c = 0.68$ nm). The crystal

Table 1 Ca/P molar ratio of various calcium phosphates [31–33]

Calcium phosphates	Abbreviations	Chemical Formula	Ca/P molar ratio	pH stability range at 25 ℃
Monocalcium phosphate monohydrate	MCPM	$Ca(H_2PO_4)_2{\cdot}H_2O$	0.5	0–2.0
Monocalcium phosphate anhydrous	MCPA	$Ca(H_2PO_4)_2$	0.5	–
Dicalcium phosphate dihydrate (brushite)	DCPD	$CaHPO_4{\cdot}2H_2O$	1.0	2.0–6.0
Dicalcium phosphate anhydrous (monetite)	DCPA	$CaHPO_4$	1.0	–
Octacalcium phosphate	OCP	$Ca_8(HPO_4)_2(PO_4)_4{\cdot}5H_2O$	1.33	5.5–7.0
alpha-Tricalcium phosphate	α-TCP	$\alpha\text{-}Ca_3(PO_4)_2$	1.5	–
beta-Tricalcium phosphate	β-TCP	$\beta\text{-}Ca_3(PO_4)_2$	1.5	–
Amorphous calcium phosphate	ACP	$Ca_x H_y (PO_4)_z{\cdot}nH_2O$ ($n = 3$–4.5, 15–20% H_2O)	1.2–2.22	~5 to 12
Calcium-deficient hydroxyapatite	CDHA	$Ca_{10-x}(HPO_4)_x(PO_4)_{6-x}(OH)_{2-x}$ ($0 < x < 1$)	1.5–1.67	6.5–9.5
Hydroxyapatite	HA/OHAp	$Ca_{10}(PO_4)_6(OH)_2$	1.67	9.5–12
Fluorapatite	FA/FAp	$Ca_{10}(PO_4)_6F_2$	1.67	7–12
Tetracalcium phosphate (hilgenstockite)	TTCP/TetCP	$Ca_4(PO_4)_2O$	2.0	–

growth orientation follows the c-axis of the unit cell, resulting in needle-shaped nanoparticles. These needle-shaped HAs are the main composition of the bone scaffold. HA undergoes continuous and iterative replacement and repair processes in the bone. Especially, HA has an important role in maintaining the mechanical strength of bone scaffold. Brown et al. first reported the mechanical properties of HA, such as tensile strength, compressive strength, and Young's modulus [34]. However, they only measured the mechanical properties of HAs in bulk-scale which may contain a lot of pores. There are only few studies related to the mechanical properties of HA itself. Recently, Yoon et al. reported a novel method to measure the mechanical property of HA itself using the atomic force microscopy (AFM) nanoindentation technique [12]. It should be noted that they first confirmed Young's modulus of single HA nanoparticles. HA undergoes continuous and iterative replacement and repair processes in the bone. In addition, it can be used as a pathway for various nutrients. Therefore, there are different pore structures that can aid in cell proliferation and nutrient transport [35–38]. For example, nanopore-induced HA scaffolds which show a similar size of pores in natural bones promoted cell proliferation and differentiation rates. While macropores involved in bone formation help to increase the migration of osteoblasts and osteocytes, which further promotes osteogenesis and tissue mineralization. Micropores also act as pathways, increasing angiogenesis and nutrient transport during bone regeneration [39–42]. Table 1 shows the different functions performed by different pore sizes in HA [43]. Over the past few decades, several studies have examined the effects of different pore structures in HA [44–46].

2.3 Biological properties of HA

HA has good osteogenic potential, as it is known to have proper biocompatibility and osteoconductivity with natural bone. The use of HA can help promote bone regeneration and suppress the inflammatory or other reactions to a foreign body that occur when using other artificial substances, resulting in minimized cytotoxicity [24, 47]. It is generally known that the biological affinity for bone depends on the amount of HA contained in the scaffold after implantation [48]. Juhasz et al. reported on the biological activity of HA when used as a filler in nanocomposite hydrogels [49]. They found that cellular activity increased as the concentration of HA increased up to 10 wt% in the hydrogel matrix. In addition, HA-based scaffolds have shown excellent biocompatibility, which is why several researchers and engineers are currently using HA in bone tissue engineering [50, 51]. However, HA has significant weaknesses in these applications owing to its poor mechanical properties and slow degradation properties [30]. Therefore, to improve the mechanical properties, many metals or metal alloys are used as bone graft material, with their surfaces coated with HA to increase biocompatibility [52]. Wang et al. fabricated an HA-coated magnesium alloy implant [53]. They showed that the HA coating not only increased the corrosion resistance of the Mg surface by up to 25 times but also enhanced the attachment and growth rate of cells. The problem of slow degradation with HA can be overcome using a metal-ion-substituted HA. Gritsch et al. reported on the use of copper and strontium-substituted HA scaffolds with chitosan [54]. They found that the fast release of copper in the HA led to an antibacterial effect, while the slow release of strontium guaranteed long-term bone regeneration (Table 2).

3 Fabrication methods of HA

Synthetic HA continues to be of great interest in bone tissue engineering applications owing to its high biocompatibility and bioactivity resulting from its chemical similarity with the mineral compounds of human bone [55]. However, as the osteoconductive and osteoinductive properties of HA are highly determined by its physiochemical properties, several researchers have been actively reporting on various methods of synthesizing HA over the past few decades. [56–62]. Importantly, the characteristics of HA, such as phase purity, crystallinity, stoichiometry, size, and shape, can be changed through the use of different synthesis methods. There are three types of methods used for HA synthesis: (1) dry synthesis, (2) wet synthesis, and (3) high-temperature synthesis.

3.1 Dry synthesis

Dry HA synthesis methods do not require the use of solvents. These methods do not significantly change the properties of the obtained HA powder and are widely used for the mass production of HA powder [24, 63]. In addition, most dry HA synthesis methods do not require precise control of the process parameters, resulting in low production costs. The dry methods can be further divided into two types: solid-state and mechanochemical methods.

Table 2 Function according to pore size in HA bone

Pore size (μm)	Function
< 1	Protein interaction, responsible for bioactivity
1–20	Cell attachment, orientation of cellular growth (directionally)
100–1000	Cellular growth and bone ingrowth
> 1000	Shape and functionality of implant

3.1.1 Solid-state methods

A solid-state reaction is a decomposition reaction in which a mixture of solid reactants is heated to produce new solids and gases [64]. In terms of HA synthesis, the solid-state method involves a simple reaction of chemical precursors containing calcium and phosphate. This method requires high temperatures to ensure the solid diffusion of ions from the precursor reagents (calcium and phosphate). Pramanik et al. reported on the synthesis of hexagonal-structured HA using a solid-state method [65]. They used calcium oxide (CaO) and phosphorus pentoxide (P_2O_5) as precursors for HA synthesis. Through X-ray diffraction (XRD) patterns, they found that the synthesized HA was a good match for monetite HA ($CaPO_3(OH)$) and calcium-deficient HA ($Ca_9(HPO_4)(PO_4)_5(OH)$). Konnawoot et al. also synthesized HA using a solid-state method [66]. Calcium carbonate ($CaCO_3$) was used as the calcium precursor and ammonium dihydrogen phosphate ($NH_4H_2PO_4$) was used as the phosphate precursor for synthesis. They investigated different calcination temperatures and reaction times required for the synthesis of high-purity HA. They found that HA with the highest purity was obtained at a calcination temperature of 1250 °C for 2 h. In a follow-up study, Arkin et al. used a different calcination temperature of 1300 °C for 7 h [67].

However, solid reactions generally produce a secondary phase in the final product, which leads to the formation of an inhomogeneous HA powder [68]. This suggests that long-term calcination is required to homogenize the system configuration. This is a major drawback in biomedical engineering applications, where precise control of the properties of the product is very important. To solve this issue, some researchers have further investigated the fundamental mechanisms of solid-state methods for HA synthesis. Recently, Javadinejad et al. systemically investigated the mechanisms of the solid-state reaction to produce HA under non-isothermal conditions [69]. They observed that non-isothermal conditions allowed the study of the kinetics of solid-state reactions better than isothermal conditions. They performed a kinetic analysis of the solid-state reactions using an iso-conversational method, and the kinetic parameters were calculated for four different heating rates. As a result, they were able to demonstrate that the formation of HA does not depend on the heating rate but is related to increasing temperature.

3.1.2 Mechanochemical method

Mechanochemical synthesis is a suitable method for producing nanomaterials, including ceramic powders, that require high-temperature systems because they do not use heat to cause chemical reactions [70, 71]. The reaction process includes the coupling of mechanical and chemical phenomena on a molecular scale by graining and mixing microstructures involving repeated fracture and deformation of nanoparticles during collision [72, 73]. In particular, milling techniques, such as ball milling and planetary milling, are often used in this method. Several studies have shown that milling methods can influence various parameters, including impact compression, local temperature, and diffusion processes resulting increase in crystallinity of HA [74–76]. This method is typically performed in sealed containers made of materials such as stainless steel, zirconia, and agate to diminish the effects of air and moisture [77]. Fathi et al. reported on the synthesis of fluoridated hydroxyapatite via mechanical alloying [78]. Calcium hydroxide ($Ca(OH)_2$), phosphorus pentoxide (P_2O_5), and calcium fluoride (CaF_2) were mechanically mixed using planetary mills with zirconia vials and balls. They studied the effects of various milling times (15, 30, and 60 min and 2, 4, 6, 8, 10, and 15 h) with a constant ball to HA powder weight ratio (35:1). Their XRD analysis demonstrated that the $Ca(OH)_2$ phase disappeared after milling for 15 min and the CaF_2 phase was removed after milling for 30 min. This suggests that apatite formation began at this point. As a result, they were able to demonstrate that the complete formation of fluorapatite ($Ca_{10}(PO_4)_6F_2$), with sizes ranging from 35 to 65 nm, occurred after milling for 6 h. In addition, Shue et al. synthesized HA by mechanical milling of dicalcium phosphate dihydrate ($CaHPO_4{\cdot}2H_2O$), calcium carbonate ($CaCO_3$), and urea using planetary milling with zirconia balls [79]. They found that the expected XRD pattern for HA appeared after 1 h of milling. However, the characteristic peaks in the XRD became wider when the milling time was increased to 24 h. The broadening of the XRD peaks suggests a decrease in crystallinity, which can be attributed to the formation of carbonated HA. Recently, Dinda et al. reported on the mechanochemical synthesis of nanocrystalline HA using six different powder mixtures containing monocalcium phosphate monohydrate ($Ca(H_2PO_4)_2{\cdot}H_2O$), CaO, $Ca(OH)_2$, and P_2O_5 [80]. They systematically investigated the reaction kinetics of HA phase formation during ball milling and found that the mechanochemical reaction rate between $Ca(H_2PO_4)_2{\cdot}H_2O$ and $Ca(OH)_2$ was very fast compared to other precursors. Sadat-Shojai et al. reported that mechanochemical methods can produce well-defined HA structures compared to particles produced by solid-state methods [24]. They first summarized how several factors in mechanochemical methods affected the HA produced, including milling speed, milling time, and the mass ratio of the powder to balls. In addition, they described how prolonged milling times generally increased crystallinity and decreased the particle size of HA.

3.2 Wet synthesis

The wet synthesis method uses aqueous solutions during the HA synthesis process. There are three common types of wet synthesis: chemical precipitation, hydrothermal synthesis, and hydrolysis. These methods are currently used for the synthesis of nanostructured and ordered HA particles [81–83]. In particular, wet synthesis methods are very suitable for adjusting the shape and average size of the resulting HA powder. However, they also have the disadvantage of producing HA with low crystallinity because of the low processing temperatures [24].

3.2.1 Chemical precipitation

The chemical precipitation method is one of the most extensively used techniques for HA synthesis. This method is used because it is possible to produce a large amount of HA at a reasonable cost [66]. Chemical precipitation methods generally involve several steps (see Fig. 1). First, reagents containing calcium and phosphate are mixed, with $Ca(OH)_2$ or calcium nitrate acting as the Ca^{2+} source and orthophosphoric acid or di-ammonium hydrogen phosphate acting as the PO_4^{3-} source. Next, the mixture is adjusted to ensure an alkaline pH, and the temperature range is set between room temperature and the boiling point of water [84, 85]. Finally, the solution is stirred to age it, and the precipitates are then washed, filtered, dried, and crushed to form a powder [24]. In chemical precipitation methods, the morphological properties (shape and size), stoichiometry, specific surface area, and crystallinity of the synthesized HA are significantly affected by several parameters such as the temperature, calcination, pH, reagent addition rate, and reaction time [62, 86–89]. For example, Mobasherpour et al. investigated the effect of reaction temperature on HA synthesis [89]. They found that HA particles gradually increased in size when the reaction temperature was increased from 100 to 1200 °C. They also showed that the hexagonal-dipyramidal phase of these synthesized HAs was not transformed to other calcium phosphate phases until a temperature of 1200 °C was reached. Afshar et al. investigated the effects of several parameters, including pH, atmospheric control, adding extra acid solution, and stirring speed [87]. $Ca(OH)_2$ and phosphoric acid were used as reagents for the HA synthesis. A mixture of these reagents was heated to 40 °C and stirred vigorously for 1 h. After adjusting the pH, the solution was kept overnight to obtain the HA precipitate. Using scanning electron microscopy (SEM), they found that the synthesized HA had a rod-like morphology with an average length of 200 nm and a diameter of 50 nm. They observed that the amount of Ca in the HA decreased as the pH decreased. Recently, Yelten et al. systematically investigated the effects of certain parameters, such as reaction temperature, acid addition rate, and heat-treatment temperature, on HA synthesis [62]. They showed that the HA precipitates had a spherical morphology with all the parameters tested. Most importantly, they showed that heat treatment at 1250 °C produced sharper peaks in the XRD results, indicating a more crystalline structure compared to the samples heat treated at 950 °C.

Most previous studies found that the pH of mixtures containing calcium and phosphate sources was important in determining the amount of HA produced. However, the mass production of HA has limitations in implementation, such as the coordination of certain synthesis parameters for chemical precipitation. Erkoc et al. recently proposed a continuous semi-batch synthesis process using a vortex reactor [90]. They showed that this system can be used to obtain pure phase HA in mass production. However, there is a chance that the characteristics of the HA synthesized by the mass-produced chemical precipitation method may deteriorate in terms of purity and crystallinity. Thus, further studies should be conducted to ensure the purity of the HA produced.

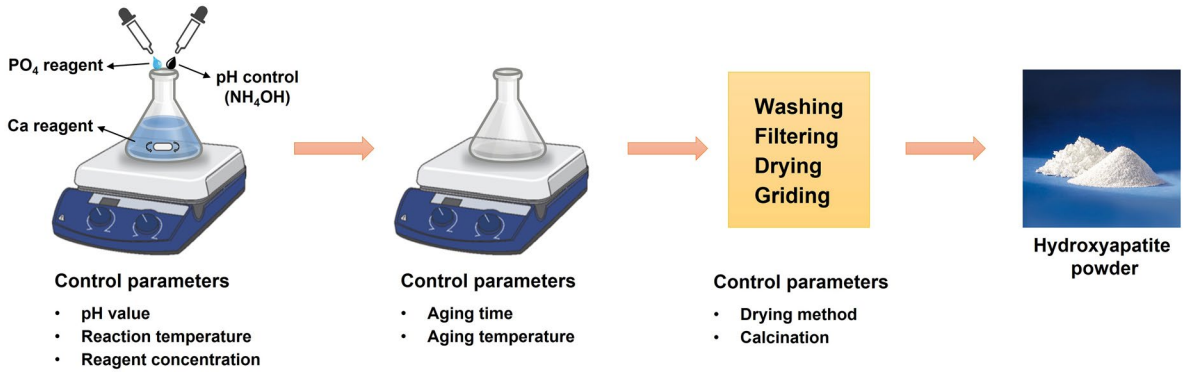

Fig. 1 Illustration of chemical precipitation process for synthesis of hydroxyapatite (HA)

3.2.2 Hydrothermal method

Hydrothermal synthesis involves chemical precipitation that occurs at high temperatures and pressures. [91, 92]. The main reactions require high temperature and high-pressure conditions, such as in an autoclave. In the early stages of this process, calcium and phosphate precursors are mixed. The addition of surfactants that can be used as templates or chemical agents, such as urea, can help control not only morphology but also nucleation and crystal growth at adjusted pH and elevated temperature and pressure. Zhang et al. described a hydrothermal method for HA synthesis [93]. Calcium chloride ($CaCl_2$) and phosphoric acid were used as the calcium and phosphate reagents, respectively. They found that rod-shaped HA with 80 nm in length and 15 nm in width was obtained by this hydrothermal method at 100 °C after 10 h. Nagata et al. also reported on a hydrothermal method using calcium nitrate tetrahydrate and di-ammonium hydrogen phosphate for HA synthesis [94]. After varying the synthesis temperature and pH conditions, they found that pure crystalline HA was obtained at pH 10 for various temperatures (25, 60, 120, or 180 °C). The XRD patterns of the synthesized HA had sharper peaks at higher temperatures, suggesting a greater degree of crystallinity.

3.2.3 Hydrolysis method

The hydrolysis method is achieved through water molecules breaking one or more chemical bonds by ionic diffusion. It is a low-temperature process carried out in an aqueous solution with different phases classified as non-stoichiometric HA. The phase change is highly dependent on the different proportions of calcium and phosphate precursors used [25, 95]. Shih et al. reported on the synthesis of nanosized HA via hydrolysis [96]. They used cetyltrimethylammonium bromide (CTAB) as a surfactant and described its role in terms of HA size and stoichiometry. Initially, when $CaHPO_4.H_2O$ (DCPD) was used, calcium-deficient HA with a width of 50 nm and a length of 100 nm was synthesized. Subsequently, CTAB was added as a surfactant in the HA synthesis process. It was found that the synthesized HA became thinner, from 20 to 5 nm in width and 50 nm in length, when the CTAB concentration was increased from 100 to 10 mM. Almirall et al. reported on the synthesis of calcium-deficient hydroxyapatite (CDHA) during the formation of α-tricalcium phosphate (α-TCP) paste and its subsequent hydrolysis [97]. A hydrogen peroxide (H_2O_2) solution was used as the forming agent, decomposing into water and oxygen gas. They showed that the HA phase produced by the hydrolysis method was similar to the biological HA found in bone. They also showed that it was possible to control the pore size, porosity, and shape by adjusting the processing parameters, such as the concentration of H_2O_2.

3.3 High-temperature method

The high-temperature method involves a process that causes the decomposition of materials through the inflow of heat energy into the system. There are two main methods used for high-temperature synthesis: combustion and pyrolysis. It is known that energy release helps to achieve the elevated temperatures required to activate the precursors required for HA synthesis [25, 95, 98]. However, there are still issues to be addressed with this approach, such as the difficulty in controlling the processing parameters and preventing secondary agglomeration [99].

3.3.1 Combustion method

Combustion synthesis is an effective process that takes advantage of an exothermic reaction in an aqueous solution. Normally, combustion synthesis starts at a low temperature and fuels are then ignited in the aqueous solutions. Organic fuels such as hydrazine, glycine, urea, citric acid, tartaric acid, and sucrose are mainly used for combustion synthesis. It is well known that oxidants help to introduce high energy levels to the combustion reaction. Rapid cooling is an important final stage of combustion synthesis, which determines the crystalline growth of the HA produced [24, 95, 98, 100]. For example, Ayers et al. reported on the synthesis of heterogeneous calcium phosphate using a combustion method [101]. Using CaO and P_2O_5 precursors, they synthesized HA and TCP under different atmospheres, including argon, nitrogen, and carbon dioxide. Through differential scanning calorimetry analysis, they showed that an ignition temperature of 450 °C can decompose P_2O_5 into PO_3, leading to a reaction with CaO. These results suggest that combustion synthesis is a viable method for producing HA from CaO and P_2O_5 precursors. Ramakrishnan et al. also synthesized HA by a combustion method using calcium nitrate and di-ammonium hydrogen phosphate as precursors [102]. They showed that combustion synthesis could produce HA with a Ca/P ratio of 1.67. In addition, they used five fuels, urea, hydrazine, glycine, alanine, and hexamine, while investigating the effects of the metal-to-fuel ratio on HA synthesis. As a result, they were able to demonstrate that all fuels used in alcohol-mediated combustion could form the pure phase of HA.

3.3.2 Pyrolysis method

The pyrolysis method involves the thermal decomposition of the materials at elevated temperatures. As fuel is not necessary in pyrolysis methods, it is possible to continuously produce HA. The pyrolysis method is frequently accompanied by precursor spray techniques for HA synthesis [24, 99, 103]. There are two main methods of spray

pyrolysis: liquid-phase reactions, which are used to control the composition of HA, and gas-phase reactions, which are used to control its morphology. Widiyastuti et al. used two components, $Ca(OOCCH_3)_2$ and $(NH_4)_2HPO_4$, to synthesize HA via a spray pyrolysis method [104]. They used nitrogen as a carrier gas to heat a furnace to 500, 700, 900, and 1000 °C. They investigated the effects of furnace temperature on the particle size, crystallinity, and reacted fraction of the HA precursors. They found that high furnace temperatures led to the synthesis of small HA particles and the formation of a pure HA phase. An et al. synthesized HA with increased crystallinity by adding salt during the spray pyrolysis process [105]. They showed that a salt-assisted decomposition (SAD) method can form a matrix that prevents HAs from aggregating, producing HA with high dispersibility and a uniform shape. They showed that a high aspect ratio and small-sized HA could be produced at 500 °C. In addition, other studies have reported that the size and density of HA are influenced by various parameters such as precursor concentration, precursor droplet size, and pyrolysis temperature [99, 106].

4 Metal ion substitution of HA

As mentioned above, HA is widely used as a bioceramic material with a hexagonal crystal structure. This HA mainly consists of Ca^{2+} and PO_4^{3-} with a Ca/P ratio of 1.67. As HA is highly adaptable in terms of its cations, certain metal ions can substitute into HA without significantly distorting its structure. Importantly, these substituted metal ions can improve the biological properties of HA, such as osteogenesis, osteoconductivity, and angiogenesis [107]. Therefore, metal-substituted HA has received a lot of attention in the past few decades, and there have been various reports that the properties of HA can be improved. For example, several metal ions such as strontium, magnesium, zinc, silicon, copper, and sodium are continuously adapted for the fabrication of metal-substituted HA. Substitution of HA with metal ions was mostly carried out based on the original HA synthesis process, including the hydrolysis method, hydrothermal method, and wet chemical and precipitation method (see Table 3). Surprisingly, most substituted metal ions cause the enhancement of biological properties in terms of HA. We now describe the effect of each metal ion on HA in detail as a bone graft material.

Table 3 Synthesis methods of metal ion substituted hydroxyapatite and performance

Substituents	Synthesis method	Performances	Numerically enhanced performances	References
Strontium	Hydrolysis method	Cell viability and proliferation	2 times higher cell viability (SAOS-2 cell)	[108]
	Hydrothermal method	Pore volume and size	Improved drug delivery efficiency	[109]
	Sol–gel dip-coating method	Bone regeneration	1.5 times more differentiation of osteoblasts	[110]
	Hydrothermal method	Cell proliferation and osteogenesis differentiation	3 times higher cell proliferation (MC3T3-E1 cells) and 1.5 times higher ALP activity	[111]
	Hydrothermal method	Angiogenesis, osteogenesis and mechanical strength	2 times higher ALP activity (MG63 cells) 1.75 times higher mechanical strength	[112]
Magnesium	Hydrolysis method	Biocompatibility	2 times as less toxic (LDH released; MC3T3-E1 cells)	[113]
	Mechanochemical method	Cytocompatibility	Cell growth, cellular activity, and average metabolic activity (MG63 cells)	[114]
	Wet chemical precipitation and hydrothermal method	Cellular viability and proliferation	2 times higher cellular area (calvaria osteoblast cells)	[115]
Zinc	Chemical precipitation method	Biocompatibility	1.2 times of cell proliferation and 2 times of ALP activity (SAOS-2 cells)	[116]
	Wet precipitation method	Antimicrobial	5 times more *E. coli* and 6 times more *S. pasteurii*	[117]
Silicon	Solid state method	Biocompatibility	2 times higher cell growth activity	[118]
Copper	Wet precipitation method	Biocompatibility	1.2 times higher cell growth (MG63 cells)	[119]
	Hydrothermal method	Angiogenesis	More blood vessel in New Zealand rabbits	[120]
Sodium	Hydrothermal method	Osteoconductivity	10 times higher in regenerated the bone	[121]

4.1 Strontium

Strontium is a chemical element with an atomic number of 38. In general, it makes up 0.008–0.01% of our bodies. The overall concentration of strontium ions (Sr^{2+}) is related to the calcium present in the body [122], and it plays an important role in bone regeneration. For example, Sr^{2+} not only slows down the breakdown of old bone but also enhances new bone formation [123–125]. For this reason, many researchers have tried to substitute Sr^{2+} in HA to enhance cell proliferation and bone growth [126]. However, as the ionic radius of Sr^{2+} (0.118 nm) is larger than that of calcium (0.100 nm), this radius difference can induce relaxation of the lattice in surrounding atoms and cause enlargement of unit cell parameters [127]. A few researchers have attempted to solve these issues by developing specific HA synthesis methods [109, 128, 129].

Frasnelli et al. suggested an aqueous precipitation method for the synthesis of homogeneous Sr^{2+}-substituted HA (Sr-HA) [108]. They produced stable Sr-HA nanopowders with different concentrations of Sr^{2+} ions varying from 0 to 100 mol%. Importantly, they found a specific point in the HA lattice where the complete dissolution of Sr^{2+} occurred. They showed that the size of Sr-HA depends on the concentration of Sr^{2+} (see Fig. 2a). Furthermore, they demonstrated that stable Sr-HA promoted osteosarcoma cell line SAOS-2 viability and proliferation (Fig. 2b). Park et al. also reported a novel synthesis method for Sr^{2+}-substituted HA (Sr-HA) via a hydrothermal reaction method using poly(aspartic acid) (PASP) as a template [109]. They controlled various parameters, namely reaction time, amount of L-aspartic

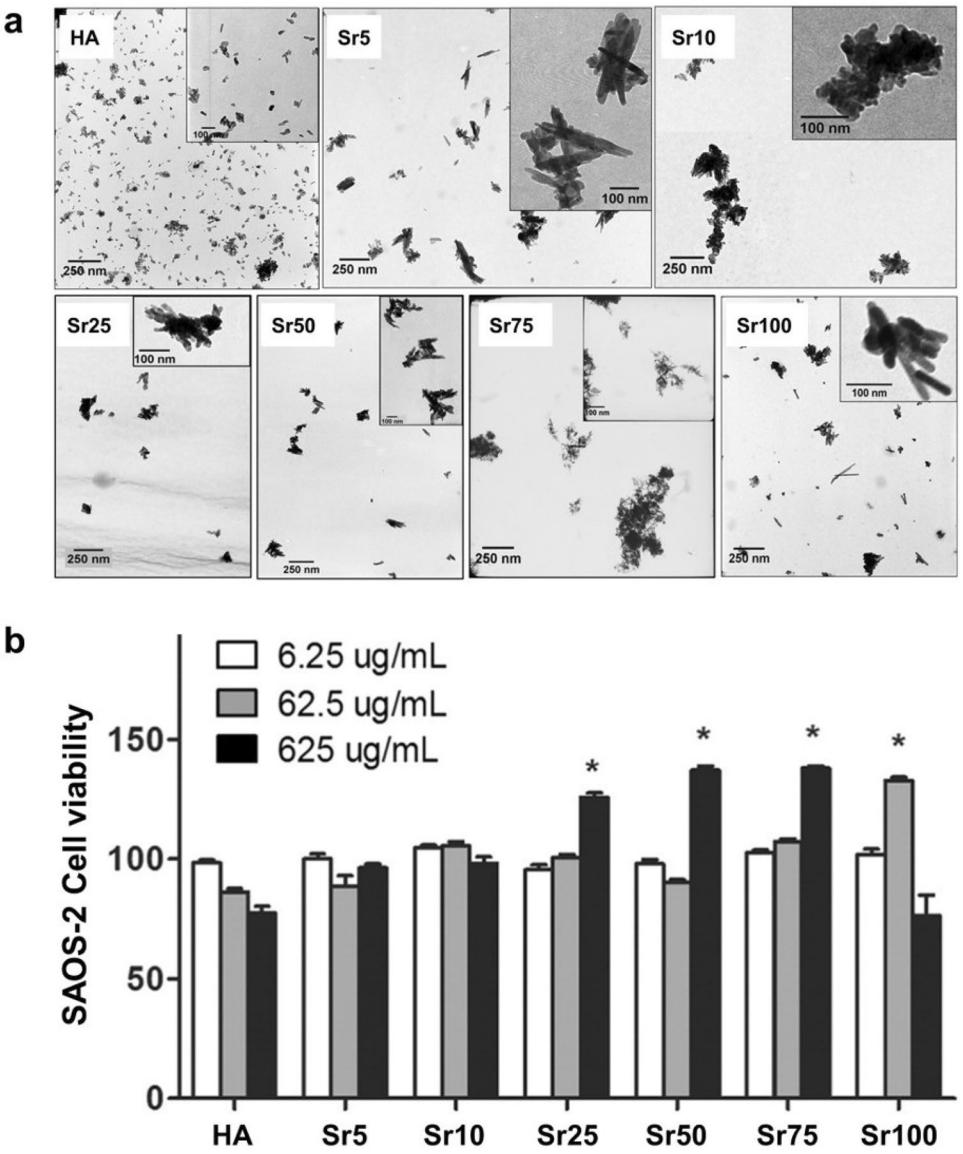

Fig. 2 **a** Transmission electron microscopy images of HA and Sr^{2+}-substituted HA (Sr-HA) according to the concentration of Sr^{2+}. **b** SAOS-2 cell viability when treated with HA and Sr-HA with different concentrations of Sr^{2+} ($p^* < 0.05$) [108]

acid (L-Asp), and the ratio of Sr ions. They found that L-Asp could influence the morphology and other properties of the produced Sr-HA. In addition, they showed that the amount of Sr^{2+} substitution changed the size, morphology, and surface area of the Sr-HA, and that a molar ratio (Sr/[Ca + Sr]) of 0.25 showed the highest efficiency when used as a drug delivery agent.

Several studies have shown enhanced biological effects, such as bone formation, angiogenesis, and osteoimmunization, of Sr-HA coated on other substrates. Li et al. reported on the fabrication of bioactive bone graft materials by coating a true bone ceramic (TBC) substrate with Sr-HA [110]. They adapted a sol–gel dip-coating method to uniformly coat Sr-HA on the TBC substrate. They showed that TBC-modified Sr-HA significantly enhanced the adhesion, proliferation, and osteogenic differentiation of MC3T3-E1 osteoblasts in vitro. Furthermore, they found that the TBC coated with 10% Sr-HA caused greater bone formation compared with raw TBC after 12 weeks of implantation. They also reported that Sr-HA combined with poly(propylene fumarate) (PPF) as a polymeric scaffold improved cell proliferation and osteogenesis differentiation [111]. Geng et al. described the fabrication of titanium (Ti)-coated Sr-HA via a hydrothermal method. They also used biodegradable miR-21 to coat Ti-coated Sr-HA. They showed that Sr-HA and miR-21 have a synergistic effect on bone formation and osseointegration [112].

4.2 Magnesium

Magnesium is a mineral that is important for the bones and teeth. It makes up approximately 0.5–1.5 wt% of our bodies. Most significantly, it is well known that magnesium ions (Mg^{2+}) play an important role in osteogenesis. In addition, magnesium deficiency can lead to bone loss and fractures [130]. Several trials have attempted to incorporate magnesium into HA to enhance bone formation. For example, even a small amount of Mg doped in HA has been reported to improve bioactivity [131, 132]. In the past, researchers have actively developed methods for the synthesis of Mg-substituted HA (Mg-HA). However, it is difficult to replace Ca^{2+} with Mg^{2+}, because there is a difference in radius between them (0.28 Å), resulting in the distortion of the HA lattice (see Fig. 3a) [133].

Chaudhry et al. first used a continuous hydrothermal flow synthesis method for the synthesis of Mg-HA [134], using a stream of superheated water to effectively nucleate and crystallize Mg-HA. They showed that as the degree of substitution from Ca^{2+} to Mg^{2+} increased, the Mg-HA became ever more amorphous, resulting in an increase in the surface area, as determined by Brunauer–Emmett–Teller (BET) analysis (see Fig. 3b). Farzadi et al. also reported on the fabrication of Mg-HA via a wet chemical precipitation method [135].

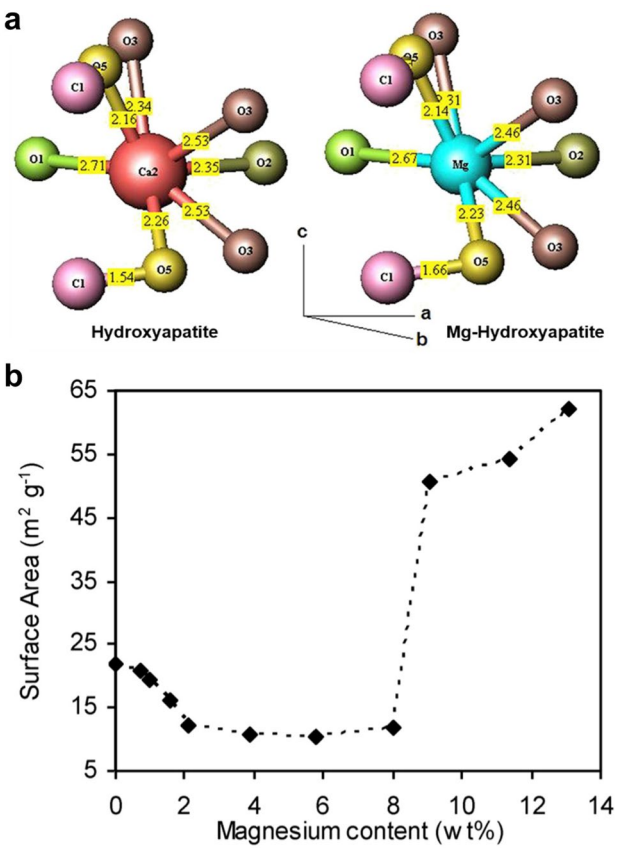

Fig. 3 **a** 3D illustration of HA and Mg^{2+}-substituted HA (Mg-HA) [133]. **b** BET surface area of Mg-HA with different concentrations of Mg^{2+} [134]

They investigated the effect of Mg^{2+} incorporation into stoichiometric Mg-HA powder. Their XRD results showed that the substitution of Mg^{2+} for Ca^{2+} in the HA lattice resulted in an increase in the lattice and a decrease in the c lattice parameters by 0.0966% and 0.2964%, respectively. However, they found that the incorporation of Mg^{2+} did not change the size of HA using transmission electron microscopy (TEM) analysis. Most importantly, they showed that the incorporation of Mg^{2+} into the HA lattice did not change the high-temperature phase stability. Thus, they concluded that the calcium phosphate phase could remain as a single-phase hexagonal structure of HA in both HA and Mg-HA.

A few studies have investigated the effect of Mg-HA on cell proliferation. Tamimi et al. examined the biological properties of Mg-HA [113]. They showed the excellent biocompatibility of Mg-HA with osteoblasts and bone marrow cell cultures. In addition, they found that certain Mg-HA phases promoted osteogenic activity in vivo. Ewald et al. compared calcium-deficient hydroxyapatite (CDHA, $Ca_9(PO_4)5HPO_4(OH)$) and Mg-HA in terms of osteoblast activity [114]. They showed that the cytocompatibility of Mg-HA was much higher than that of CDHA, and this

result could also be observed in the initial stages of cell surface contact by examining the metabolic state and protein expression. Andres et al. also fabricated bone mimetic HA by substituting magnesium for calcium to improve bone repair properties [115]. They used an aqueous wet chemical precipitation and hydrothermal treatment method to obtain Mg-HA. They showed that the synthesized Mg-HA had a large area of cellular extension, which could lead to an increase in in vitro cellular viability, spreading, and proliferation compared to CDHA.

4.3 Zinc

Zinc is an essential nutrient, which enhances the immune system and metabolic functions. Typically, most zinc ions (Zn^{2+}) are present in the muscles, while they also exist in human bone [136]. Furthermore, it is known that Zn^{2+} can act as an agent for cell growth, division, protein production, enzyme reactions, and DNA synthesis. Yamaguchi et al. first showed that Zn^{2+} is a trigger for alkaline phosphatase activity and DNA synthesis [137]. As zinc is able to promote bone regeneration, several studies used Zn^{2+} as a substitute ion when producing HA. Zinc is of great interest because it can cause a reduction in bone resorption and has an antibacterial effect. In general, HA cannot inhibit bacterial attachment to its surface under biological conditions. Therefore, it is important to find a way to prevent bacterial growth on the surface of HA in bone tissue engineering applications.

Ergun et al. first fabricated Zn^{2+}-substituted HA (Zn-HA) via high-temperature sintering [138]. They characterized Zn-HA with different concentrations of Zn^{2+} via XRD and SEM. Miyaji et al. symmetrically investigated how the fraction of Zn^{2+} can change the HA phase from the amorphous to the amorphous/parascholzite phase [139]. They described how the difference in the ionic radii of Zn^{2+} (0.074 nm) and Ca^{2+} (0.099 nm) determines the lattice parameters of HA. For example, the lattice parameter c decreases with an increasing Zn^{2+} fraction. In addition, the lattice parameter increases with the Zn^{2+} fraction because of the amount of H_2O substituted into the OH sites of the HA structure (see Fig. 4a). Li et al. also found that zinc-substituted HA caused variations in the HA structure, including changes in crystallinity due to the difference in ionic radius between Zn^{2+} and Ca^{2+} [140]. On the other hand, Zn^{2+} restrained the growth of substituted HA crystals, resulting in a reduction in the thermal stability of Zn-HA. Zhong et al. first suggested a fast synthesis method for Zn-HA [141]. They used citrate ions to achieve this as they caused additional interactions with Zn^{2+} during the recrystallization process. As a result, they were able to obtain Zn-HA with a length of 29 nm and a thickness of 3–5 nm within 15 min. They found negligible stability issues for Zn-HA synthesized via a rapid synthesis method.

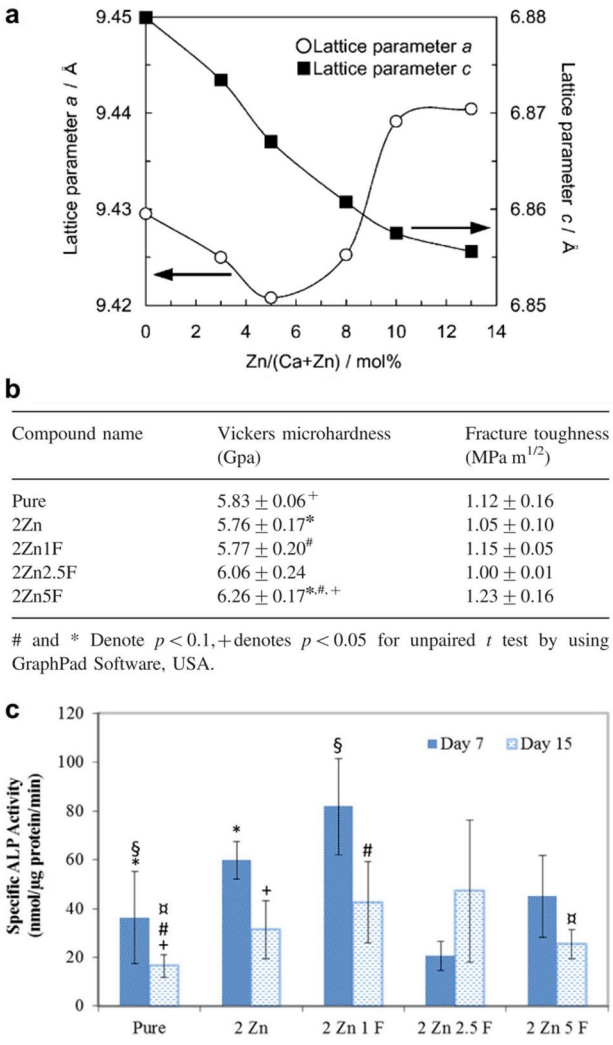

b

Compound name	Vickers microhardness (Gpa)	Fracture toughness (MPa $m^{1/2}$)
Pure	$5.83 \pm 0.06^{+}$	1.12 ± 0.16
2Zn	$5.76 \pm 0.17^{*}$	1.05 ± 0.10
2Zn1F	$5.77 \pm 0.20^{\#}$	1.15 ± 0.05
2Zn2.5F	6.06 ± 0.24	1.00 ± 0.01
2Zn5F	$6.26 \pm 0.17^{*,\#,+}$	1.23 ± 0.16

and * Denote $p < 0.1$, + denotes $p < 0.05$ for unpaired t test by using GraphPad Software, USA.

Fig. 4. **a** Lattice parameters a and c for zinc-substituted HA (Zn-HA) according to Zn fraction [139]. **b** Mechanical properties of Zn^{2+} and F^{-} co-doped HA. **c** Alkaline phosphatase (ALP) activities of the cells treated with bare HA (pure) and Zn^{2+} and F^{-} co-doped HA samples [116]

Uysal et al. first characterized the effect of Zn^{2+} in Zn-HA in terms of its mechanical and biological properties [116]. They additionally doped a fluoride ion (F^{-}) to substitute for OH in the HA structure. They demonstrated that co-doping with Zn^{2+} and F^{-} improved the microhardness and fracture toughness compared to bare HA (see Fig. 4b). In addition, they showed that the alkaline phosphatase (ALP) activities of the Saos-2 cells increased with Zn-HA containing 1 mol% F^{-} compared to bare HA (see Fig. 4c). Consequently, they were able to find an optimum ratio of Zn^{2+} to F^{-} for use in bone graft materials. Thian et al. also demonstrated that Zn-HA has good Saos-2 cell viability and excellent protein expression compared to bare HA [142]. Recently, a few studies have demonstrated the enhanced antibacterial effect of Zn-HA. Irfan et al. showed the antibacterial properties of

Zn-HA, which showed good antibacterial effects against both *E. coli* and *S. pasteurii* compared to bare HA [117].

4.4 Silicon

Although silicon exists in small amounts in the body (0.0015%), it is well known that silicon plays an important role in the early stages of bone formation [143, 144]. It has been reported that silicon is highly concentrated in immature bone, and its content decreases with increasing calcium content in mature bone [145]. In addition, silicon may influence bone regeneration, mineralization, and bioactivity in human bone osteoblasts. Importantly, silicon has a significant effect on bone formation, independent of vitamin D, through its association with a hormone involved in bone formation [143]. Therefore, a few researchers have created silicon-substituted HA (Si-HA) for application in bone tissue engineering. Bang et al. studied the fabrication of silicon-substituted carbonate HA (Si-CO_3 HA) [146]. They found that Si-CO_3 HA decreased the powder crystallinity and promoted ion release, resulting in better solubility compared to bare carbonate HA. Tsalsabila et al. reported on the microwave-assisted synthesis of Si-HA with different concentrations of silicon (0, 0.4, 0.8 and 1.2 wt%) [147]. They found that microwave irradiation helped to shorten the synthesis process of Si-HA, as there was no need for aging. They showed that this method could successfully reduce the synthesis steps required for Si-HA, which has a Ca/P ratio of 1.68. However, to the best of our knowledge, few studies have investigated the biological effects of Si-HA on bone formation. Thian et al. indirectly investigated the biological effect of Si-HA on the surface of a Ti substrate with a view to its use as an implant material [118]. They coated Si-HA on a Ti substrate at different concentrations and found that all Si-HA samples showed excellent growth promotion of osteoblast-like (HOB) cells compared to bare HA (see Fig. 5a). In addition, they found that the actin cytoskeleton on Si-HA produced long, distinct microfilament alignment compared to bare HA (see Fig. 5b).

4.5 Copper

Copper (Cu) is an important element involved in human metabolism. In bone graft materials, Cu is known to play a crucial role in bone maintenance. For example, Cu deficiency has been reported to reduce bone mineral content and bone strength. In addition, copper ions (Cu^{2+}) can act as cofactors for various enzymes such as lysyl oxidase, which is related to the cross-linking of collagen fibrils [148]. This indicates that Cu^{2+} is related to bone mineralization. Therefore, Cu^{2+} is currently being used in the development of bone graft materials, including HA.

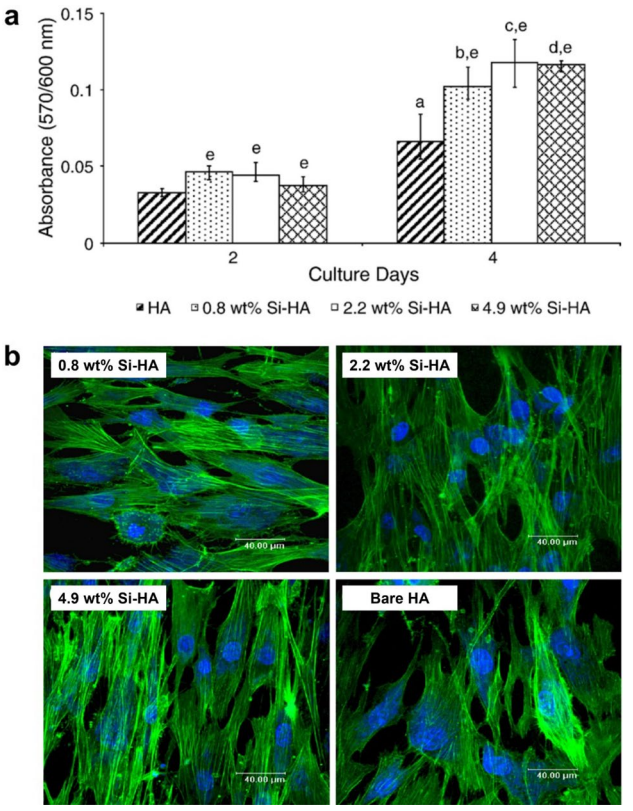

Fig. 5 **a** Growth activity of human osteoblast-like (HOB) cells at a different culturing time. $^{a}p<0.05$: growth activity was higher on HA between groups; $^{b}p<0.05$: growth activity was higher on 0.8 wt% Si-HA between groups; $^{c}p<0.05$: growth activity was higher on 2.2 wt% Si-HA between groups; $^{d}p<0.05$: growth activity was higher on 4.9 wt% Si-HA between groups; $^{e}p<0.05$: growth activity was higher on Si-HA than bare HA within groups. **b** Immunostained images of nuclear DNA (blue) and actin cytoskeleton (green) in HOB after 1 day [118]

Shanmugam et al. reported on the fabrication of Cu-substituted HA (Cu-HA) via a precipitation method [149]. In addition, they used F^- to substitute into the OH sites of the HA structure. They observed a secondary phase (β-TCP) with an increase in Cu^{2+} content from 0.5 to 2 in $Ca_{10-x}Cu_x(PO_4)_6(OH/F)_2$. Importantly, they demonstrated that Cu-HA has an increased antibacterial effect compared to bare HA against *S. aureus*, *E. coli*, and *C. albicans* (see Fig. 6a). Yu. Nikitina et al. also fabricated Cu-HA through a precipitation method and demonstrated the antimicrobial activity of Cu-HA with various Cu content [119]. Furthermore, they found that a certain Cu content increased cell viability compared to that of bare HA. In addition, a few studies have demonstrated the effect of Cu-HA through in vivo testing. Elrayah et al. described the preparation of micro/nanostructured Cu-HA for bone tissue engineering [120]. They fabricated Cu-HA scaffolds with varying Cu content. As the Cu content increased, the surface structure of Cu-HA changed from smooth to spherical, flower-like,

a

Compound	Antimicrobial ratio (%)		
	S. aureus	*E. coli*	*C. albicans*
$Ca_5(PO_4)_3OH$ (HAP)	48.5	82.6	62.4
$Ca_{9.95}Cu_{0.05}(PO_4)_6(OH)_2$ (Cu05OH)	66.1	25	80.1
$Ca_{9.9}Cu_{0.1}(PO_4)_6(OH)_2$ (Cu1OH)	89.0	28.5	74.5
$Ca_{9.85}Cu_{0.15}(PO_4)_6(OH)_2$ (Cu15OH)	73.2	30	73.0
$Ca_{9.8}Cu_{0.2}(PO_4)_6(OH)_2$ (Cu2OH)	98.4	32.5	82.3
$Ca_{9.75}Cu_{0.25}(PO_4)_6(OH)_2$ (Cu25OH)	98.9	65	65.2
$Ca_{9.5}Cu_{0.5}(PO_4)_6(OH)_2$ (Cu5OH)	98.9	82.5	72.3

b

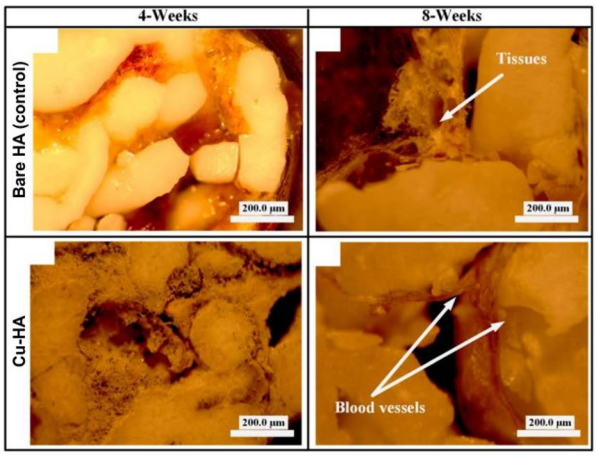

Fig. 6 **a** Comparison of the antibacterial effect from bare HA and Cu-HA with different Cu contents [149]. **b** Optical microscopic images of bare HA (control) and Cu-HA scaffold 4 weeks and 8 weeks after implantation [120]

and nanocrystals. They implanted flower-like Cu-HA subcutaneously into the skeleton skin of New Zealand rabbits. They found that the Cu-HA scaffold resulted in the formation of more blood vessels compared to that of bare HA (see Fig. 6b). It should be noted that this is the first study to demonstrate the angiogenic ability of Cu-HA through in vivo testing.

4.6 Sodium

Sodium ions (Na^+) are essential nutrients necessary for hearing ability and metabolic function [150]. It is known that the ionic radius of Na^+ (0.102 nm) is very similar to that of Ca^{2+} (0.100 nm). Therefore, researchers expected that the synthesis of sodium-substituted HA (Na-HA) would be much easier than for other metal ions.

However, Cho et al., who first reported the synthesis of Na-HA via the precipitation method, found instability issues for Na-HA [121]. This was attributed to the charge difference between Na^+ and Ca^{2+} ions. This system instability of Na-HA caused an accelerated release of constituent elements, such as Ca^{2+} and OH^-, resulting in a positive influence on osteoconductivity (Fig. 7). However, the number of papers on Na-HA is extremely small compared to other metal-substituted HAs, as most studies have focused on the problem of Na + for diabetes [151].

5 Summary and perspectives

In summary, the addition of metal ions not only helps to improve the physical and chemical properties of HA, but also its biological functions, such as osteogenesis, osteoconductivity, and angiogenesis. To understand the effects of metal ion substitution in HA, we first reviewed the basic properties of HA in natural bone in terms of their chemical, physical, and biological functions. We then summarized various HA synthesis methods, including: (1) dry synthesis, (2) wet synthesis, and (3) high-temperature synthesis. Importantly, all metal substituted HAs are synthesized using the original HA synthesis process. Finally, we classified representative studies on metal-substituted HAs, including Sr-HA, Mg-HA, Zn-HA, Si-HA, Cu-HA, and Na-HA. It should be noted that most metal ions lead to crystal-structured HA owing to the differences in ionic radius and charge. However, metal ions significantly improved the bone regeneration properties of HA in terms of osteoconductivity and angiogenesis. As such, it is expected that the use of metal-substituted HA will continue to be of great interest. However, there are a few issues that need to be addressed to further adapt metal-substituted HA for bone tissue engineering applications.

First, when Ca^{2+} is replaced with other metal ions in HA, there is an issue with distortion of HA crystallinity due to the difference in ionic radii. Although many researchers have chosen specific metal ions, such as Na^+, with ionic radii relatively similar to Ca^{2+} to minimize this issue [121], there are still problems with instability. Thus, it is very important to further investigate the relationship between metal ions and Ca^{2+} to produce the best possible HA structure.

Second, there is a need to perform in vivo tests to investigate the effects of metal-substituted HA in the biological environment. To the best of our knowledge, very few studies have performed in vivo testing of metal-substituted HAs. Typically, it is almost impossible to obtain accurate biological results from in vitro tests. Furthermore, as clinical trials are necessary for the practical use of metal-substituted HAs in bone tissue engineering applications, in vivo testing should be carried out beforehand.

Finally, further studies are necessary to confirm the effects of metal-substituted HAs on vasculogenesis and angiogenesis. It is well known that angiogenesis is an important factor in bone regeneration because once blood vessels are not properly formed, the growth of cells is

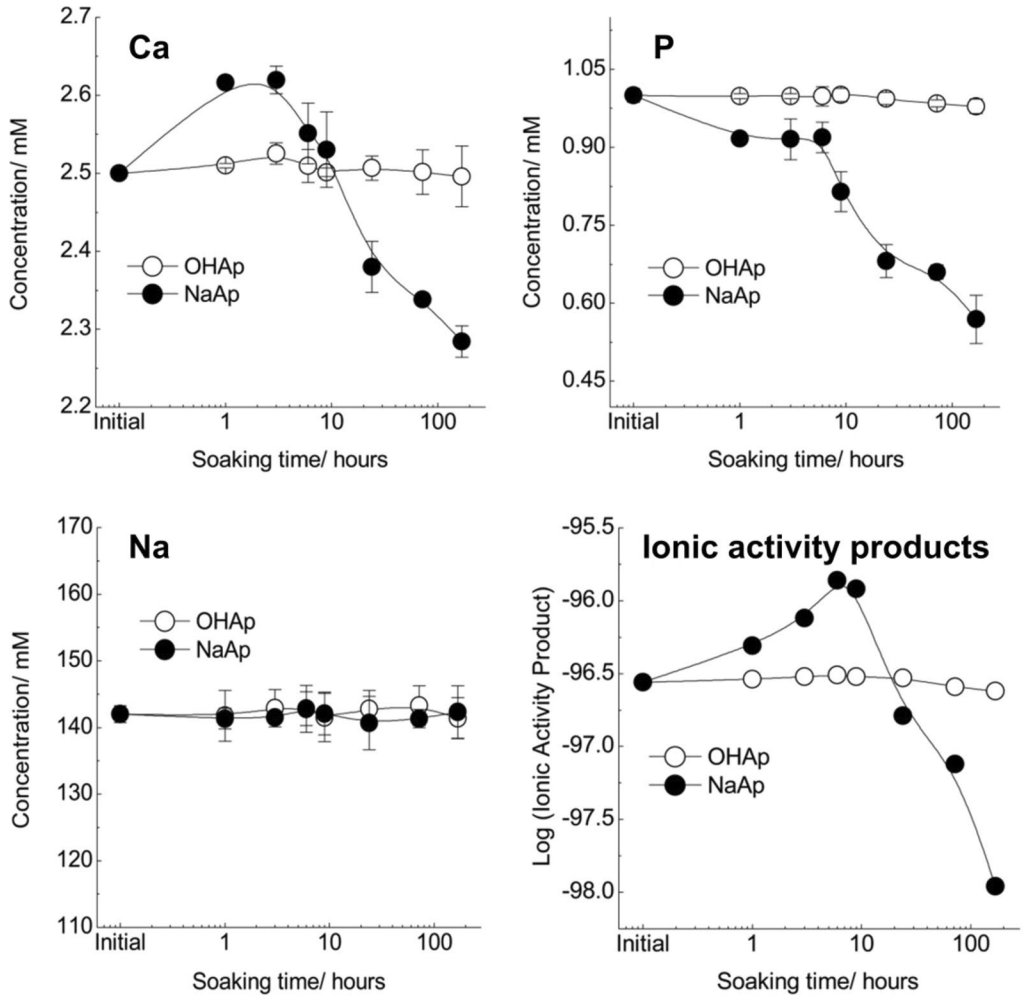

Fig. 7 Comparison of ion release concentrations for calcium (Ca), phosphorous (P), sodium (Na) and ionic activity products in HA in a simulated body fluid after soaking of bare HA (OHA) and sodium-substituted HA (NaAp) [121]

inhibited [152]. A previous study reported that metal-substituted HA enhanced angiogenic activity [120]. However, the underlying mechanism by which metal-substituted HA affects angiogenic activity has not been sufficiently investigated for the use of metal-substituted HA in future bone tissue engineering applications. If these studies continue, we believe that metal-substituted HA can be used commercially in a wide range of bone tissue engineering applications.

Funding This research was supported by grants from the National Research Foundation of Korea funded by the Ministry of Science and ICT for Bio-inspired Innovation Technology Development Project (NRF-2018M3C1B7021997) and Basic Science Research Program (NRF-2020R1A2C2006100). Dr. Jun Hyuk Heo and Mr. Si Hyun Kim appreciate the support of the National Research Foundation of Korea funded by the Ministry of Education (NRF-2022R1C1C2002823 (JHH) and NRF-2020R1A6A3A13070482 (SHK)).

Availability of data and material Not applicable.

Code availability Not applicable.

Declarations

Conflict of interest The authors declare no competing interest.

References

1. Z. Tang, Y. Tan, Y. Ni, J. Wang, X. Zhu, Y. Fan, X. Chen, X. Yang, X. Zhang, Comparison of ectopic bone formation process induced by four calcium phosphate ceramics in mice. Mater. Sci. Eng. C **70**, 1000–1010 (2017). https://doi.org/10.1016/j.msec.2016.06.097
2. Y. Deng, Y. Yang, Y. Ma, K. Fan, W. Yang, G. Yin, Nano-hydroxyapatite reinforced polyphenylene sulfide biocomposite with superior cytocompatibility and in vivo osteogenesis as a

novel orthopedic implant. RSC Adv. **7**, 559–573 (2017). https://doi.org/10.1039/c6ra25526d
3. J.H. Lee, G.S. Yi, J.W. Lee, D.J. Kim, Physicochemical characterization of porcine bone-derived grafting material and comparison with bovine xenografts for dental applications. J. Periodontal Implant Sci. **47**, 388–401 (2017). https://doi.org/10.5051/jpis.2017.47.6.388
4. T.H. Lim, J.R. Choi, D.Y. Lim, S.H. Lee, S.Y. Yeo, Preparation of fiber based binder materials to enhance the gas adsorption efficiency of carbon air filter. J. Nanosci. Nanotechnol. **15**, 8034–8041 (2015). https://doi.org/10.1166/jnn.2015.11276
5. L.F. Sukhodub, L.B. Sukhodub, A.D. Pogrebnjak, A. Turlybekuly, A. Kistaubayeva, I. Savitskaya, D. Shokatayeva, Effect of magnetic particles adding into nanostructured hydroxyapatite–alginate composites for orthopedics. J. Korean Ceram. Soc. **57**, 557–569 (2020). https://doi.org/10.1007/s43207-020-00061-w
6. B. Mohapatra, T.R. Rautray, Strontium-substituted biphasic calcium phosphate scaffold for orthopedic applications. J. Korean Ceram. Soc. **57**, 392–400 (2020). https://doi.org/10.1007/s43207-020-00028-x
7. C. Shuai, S. Li, S. Peng, P. Feng, Y. Lai, C. Gao, Biodegradable metallic bone implants. Mater. Chem. Front. **3**, 544–562 (2019). https://doi.org/10.1039/c8qm00507a
8. N. Strutynska, A. Malyshenko, N. Tverdokhleb, M. Evstigneev, L. Vovchenko, Y. Prylutskyy, N. Slobodyanik, U. Ritter, Design, characterization and mechanical properties of new Na^+, CO_3^{2-}-apatite/alginate/C60 fullerene hybrid biocomposites. J. Korean Ceram. Soc. **58**, 422–429 (2021). https://doi.org/10.1007/s43207-020-00107-z
9. J.W. Lee, S. Chae, S. Oh, S.H. Kim, K.H. Choi, M. Meeseepong, J. Chang, N. Kim, Y.H. Kim, N.E. Lee, J.H. Lee, J.Y. Choi, Single-chain atomic crystals as extracellular matrix-mimicking material with exceptional biocompatibility and bioactivity. Nano Lett. **18**, 7619–7627 (2018). https://doi.org/10.1021/acs.nanolett.8b03201
10. E. Saygili, E. Kaya, E. Ilhan-Ayisigi, P. Saglam-Metiner, E. Alarcin, A. Kazan, E. Girgic, Y.W. Kim, K. Gunes, G.G. Eren-Ozcan, D. Akakin, J.Y. Sun, O. Yesil-Celiktas, An alginate-poly(acrylamide) hydrogel with TGF-β3 loaded nanoparticles for cartilage repair: biodegradability, biocompatibility and protein adsorption. Int. J. Biol. Macromol. **172**, 381–393 (2021). https://doi.org/10.1016/j.ijbiomac.2021.01.069
11. J.H. Lee, I.H. Ko, S.H. Jeon, J.H. Chae, J.H. Chang, Microstructured hydroxyapatite microspheres for local delivery of alendronate and BMP-2 carriers. Mater. Lett. **105**, 136–139 (2013). https://doi.org/10.1016/j.matlet.2013.04.082
12. H.G. Jung, D. Lee, S.W. Lee, I. Kim, Y. Kim, J.W. Jang, J.H. Lee, G. Lee, D.S. Yoon, Nanoindentation for monitoring the time-variant mechanical strength of drug-loaded collagen hydrogel regulated by hydroxyapatite nanoparticles. ACS Omega **6**, 9269–9278 (2021). https://doi.org/10.1021/acsomega.1c00824
13. M. Park, J.C. Pyun, J. Jose, Orientation and density control of proteins on solid matters by outer membrane coating: analytical and diagnostic applications. J. Pharm. Biomed. Anal. **147**, 174–184 (2018). https://doi.org/10.1016/j.jpba.2017.07.043
14. J.H. Kim, S.H. Kim, H.K. Kim, T. Akaike, S.C. Kim, Synthesis and characterization of hydroxyapatite crystals: a review study on the analytical methods. J. Biomed. Mater. Res. **62**, 600–612 (2002). https://doi.org/10.1002/jbm.10280
15. B. Cengiz, Y. Gokce, N. Yildiz, Z. Aktas, A. Calimli, Synthesis and characterization of hydroxyapatite nanoparticles. Colloids Surf. A Physicochem. Eng. Asp. **322**, 29–33 (2008). https://doi.org/10.1016/j.colsurfa.2008.02.011
16. G.B.C. Cardoso, A. Tondon, L.R.B. Maia, M.R. Cunha, C.A.C. Zavaglia, R.R. Kaunas, In vivo approach of calcium deficient hydroxyapatite filler as bone induction factor. Mater. Sci. Eng. C **99**, 999–1006 (2019). https://doi.org/10.1016/j.msec.2019.02.060
17. R.M.G. Rajapakse, W.P.S.L. Wijesinghe, M.M.M.G.P.G. Mantilaka, K.G. Chathuranga Senarathna, H.M.T.U. Herath, T.N. Premachandra, C.S.K. Ranasinghe, R.P.V.J. Rajapakse, M. Edirisinghe, S. Mahalingam, I.M.C.C.D. Bandara, S. Singh, Preparation of bone-implants by coating hydroxyapatite nanoparticles on self-formed titanium dioxide thin-layers on titanium metal surfaces. Mater. Sci. Eng. C **63**, 172–184 (2016). https://doi.org/10.1016/j.msec.2016.02.053
18. L. Chen, Z. Wu, Y. Zhou, L. Li, Y. Wang, Z. Wang, Y. Chen, P. Zhang, Biomimetic porous collagen/hydroxyapatite scaffold for bone tissue engineering. J. Appl. Polym. Sci. **134**, 1–8 (2017). https://doi.org/10.1002/app.45271
19. S.M. Lee, H.J. Byeon, B.H. Kim, J. Lee, J.Y. Jeong, J.H. Lee, J.H. Moon, C. Park, H. Choi, S.H. Lee, K.H. Lee, Flexible and implantable capacitive microelectrode for bio-potential acquisition. Biochip J. **11**, 153–163 (2017). https://doi.org/10.1007/s13206-017-1304-y
20. E. Boanini, M. Gazzano, A. Bigi, Ionic substitutions in calcium phosphates synthesized at low temperature. Acta Biomater. **6**, 1882–1894 (2010). https://doi.org/10.1016/j.actbio.2009.12.041
21. K. Sato, Mechanism of hydroxyapatite mineralization in biological systems. J. Ceram. Soc. Japan **115**, 124–130 (2007). https://doi.org/10.2109/jcersj.115.124
22. S.H. Han, J.U. Lee, K.M. Lee, Y.Z. Jin, H. Yun, G.H. Kim, J.H. Lee, Enhanced healing of rat calvarial defects with 3D printed calcium-deficient hydroxyapatite/collagen/bone morphogenetic protein 2 scaffolds. J. Mech. Behav. Biomed. Mater. **108**, 103782 (2020). https://doi.org/10.1016/j.jmbbm.2020.103782
23. M. Vallet-Regí, J.M. González-Calbet, Calcium phosphates as substitution of bone tissues. Prog. Solid State Chem. **32**, 1–31 (2004). https://doi.org/10.1016/j.progsolidstchem.2004.07.001
24. M. Sadat-Shojai, M.T. Khorasani, E. Dinpanah-Khoshdargi, A. Jamshidi, Synthesis methods for nanosized hydroxyapatite with diverse structures. Acta Biomater. **9**, 7591–7621 (2013). https://doi.org/10.1016/j.actbio.2013.04.012
25. A. Szcześ, L. Hołysz, E. Chibowski, Synthesis of hydroxyapatite for biomedical applications. Adv. Colloid Interface Sci. **249**, 321–330 (2017). https://doi.org/10.1016/j.cis.2017.04.007
26. J. Vecstaudza, M. Gasik, J. Locs, Amorphous calcium phosphate materials: formation, structure and thermal behaviour. J. Eur. Ceram. Soc. **39**, 1642–1649 (2019). https://doi.org/10.1016/j.jeurceramsoc.2018.11.003
27. J.M. Thomann, J.C. Voegel, P. Gramain, Kinetics of dissolution of calcium hydroxyapatite powder. III: pH and sample conditioning effects. Calcif Tissue Int. **46**, 121–129 (1990). https://doi.org/10.1007/BF02556096
28. L. Pighinelli, M. Kucharska, Chitosan-hydroxyapatite composites. Carbohydr. Polym. **93**, 256–262 (2013). https://doi.org/10.1016/j.carbpol.2012.06.004
29. D.W. Hutmacher, Scaffolds in tissue engineering bone and cartilage. Biomater. Silver Jubil. Compend. **21**, 175–189 (2000). https://doi.org/10.1016/B978-008045154-1.50021-6
30. K. Rezwan, Q.Z. Chen, J.J. Blaker, A.R. Boccaccini, Biodegradable and bioactive porous polymer/inorganic composite scaffolds for bone tissue engineering. Biomaterials **27**, 3413–3431 (2006). https://doi.org/10.1016/j.biomaterials.2006.01.039
31. S.V. Dorozhkin, Calcium orthophosphates in nature, biology and medicine. Materials (Basel) **2**, 399–498 (2009). https://doi.org/10.3390/ma2020399
32. S.V. Dorozhkin, Calcium orthophosphates. J. Mater. Sci. **42**, 1061–1095 (2007). https://doi.org/10.1007/s10853-006-1467-8
33. L.C. Chow, Solubility of calcium phosphates. Monogr. Oral Sci. **18**, 94–111 (2001). https://doi.org/10.1159/000061650

34. R.I. Martin, P.W. Brown, Mechanical properties of hydroxyapatite formed at physiological temperature. J. Mater. Sci. Mater. Med. **6**, 138–143 (1995). https://doi.org/10.1007/BF00120289
35. A. Gortemaker, J.A. Jansen, NHJC, Critical reviews in oral biology & medicine: aging and bone. J. Dent. Res. **89**, 1333–1348 (2010). https://doi.org/10.1177/0022034510377791
36. C.H. Turner, Bone strength: current concepts. Ann. N. Y. Acad. Sci. **1068**, 429–446 (2006). https://doi.org/10.1196/annals.1346.039
37. S.H. Ralston, Bone structure and metabolism. Medicine (United Kingdom) **45**, 560–564 (2017). https://doi.org/10.1016/j.mpmed.2017.06.008
38. K.A. Hing, S.M. Best, W. Bonfield, Characterization of porous hydroxyapatite. J. Mater. Sci. Mater. Med. **10**, 135–145 (1999). https://doi.org/10.1023/A:1008929305897
39. A.E. Jakus, A.L. Rutz, R.N. Shah, Advancing the field of 3D biomaterial printing. Biomed. Mater. (2016). https://doi.org/10.1088/1748-6041/11/1/014102
40. A. Liu, G.H. Xue, M. Sun, H.F. Shao, C.Y. Ma, Q. Gao, Z.R. Gou, S.G. Yan, Y.M. Liu, Y. He, 3D printing surgical implants at the clinic: a experimental study on anterior cruciate ligament reconstruction. Sci. Rep. **6**, 1–13 (2016). https://doi.org/10.1038/srep21704
41. K.A. Hing, B. Annaz, S. Saeed, P.A. Revell, T. Buckland, Microporosity enhances bioactivity of synthetic bone graft substitutes. J. Mater. Sci. Mater. Med. **16**, 467–475 (2005). https://doi.org/10.1007/s10856-005-6988-1
42. C. Kim, J.W. Lee, J.H. Heo, C. Park, D.H. Kim, G.S. Yi, H.C. Kang, H.S. Jung, H. Shin, Lee JH Natural bone-mimicking nanopore-incorporated hydroxyapatite scaffolds for enhanced bone tissue regeneration. Biomater Res. **26**, 7 (2022). https://doi.org/10.1186/s40824-022-00253-x
43. G. Tripathi, B. Basu, A porous hydroxyapatite scaffold for bone tissue engineering: physico-mechanical and biological evaluations. Ceram. Int. **38**, 341–349 (2012). https://doi.org/10.1016/j.ceramint.2011.07.012
44. J. Chen, Z. Wang, Z. Wen, S. Yang, J. Wang, Q. Zhang, Controllable self-assembly of mesoporous hydroxyapatite. Colloids Surf. B Biointerfaces **127**, 47–53 (2015). https://doi.org/10.1016/j.colsurfb.2014.12.055
45. F. He, Y. Yang, J. Ye, Tailoring the pore structure and property of porous biphasic calcium phosphate ceramics by NaCl additive. Ceram. Int. **42**, 14679–14684 (2016). https://doi.org/10.1016/j.ceramint.2016.06.092
46. S. Yunoki, T. Ikoma, A. Monkawa, K. Ohta, M. Kikuchi, S. Sotome, K. Shinomiya, J. Tanaka, Control of pore structure and mechanical property in hydroxyapatite/collagen composite using unidirectional ice growth. Mater. Lett. **60**, 999–1002 (2006). https://doi.org/10.1016/j.matlet.2005.10.064
47. P. Habibovic, M.C. Kruyt, M.V. Juhl, S. Clyens, R. Martinetti, L. Dolcini, N. Theilgaard, C.A. Van Blitterswijk, Comparative in vivo study of six hydroxyapatite-based bone graft substitutes. J. Orthop. Res. **26**, 1363–1370 (2008). https://doi.org/10.1002/jor.20648
48. J.R. Woodard, A.J. Hilldore, S.K. Lan, C.J. Park, A.W. Morgan, J.A.C. Eurell, S.G. Clark, M.B. Wheeler, R.D. Jamison, A.J. Wagoner Johnson, The mechanical properties and osteoconductivity of hydroxyapatite bone scaffolds with multi-scale porosity. Biomaterials **28**, 45–54 (2007). https://doi.org/10.1016/j.biomaterials.2006.08.021
49. J.A. Juhasz, S.M. Best, W. Bonfield, Preparation of novel bioactive nano-calcium phosphate-hydrogel composites. Sci. Technol. Adv. Mater. (2010). https://doi.org/10.1088/1468-6996/11/1/014103
50. C.S. Ciobanu, S.L. Iconaru, I. Pasuk, B.S. Vasile, A.R. Lupu, A. Hermenean, A. Dinischiotu, D. Predoi, Structural properties of silver doped hydroxyapatite and their biocompatibility. Mater. Sci. Eng. C **33**, 1395–1402 (2013). https://doi.org/10.1016/j.msec.2012.12.042
51. F.J. O'Brien, Biomaterials & scaffolds for tissue engineering. Mater. Today **14**, 88–95 (2011). https://doi.org/10.1016/S1369-7021(11)70058-X
52. J. Biggemann, P. Müller, D. Köllner, S. Simon, P. Hoffmann, P. Heik, J.H. Lee, T. Fey, Hierarchical surface texturing of hydroxyapatite ceramics: influence on the adhesive bonding strength of polymeric polycaprolactone. J. Funct. Biomater. (2020). https://doi.org/10.3390/JFB11040073
53. A. Jaafar, C. Hecker, P. Árki, Y. Joseph, Sol-gel derived hydroxyapatite coatings for titanium implants: a review. Bioengineering **7**, 1–23 (2020). https://doi.org/10.3390/bioengineering7040127
54. L. Gritsch, M. Maqbool, V. Mouriño, F.E. Ciraldo, M. Cresswell, P.R. Jackson, C. Lovell, A.R. Boccaccini, Chitosan/hydroxyapatite composite bone tissue engineering scaffolds with dual and decoupled therapeutic ion delivery: copper and strontium. J. Mater. Chem. B **7**, 6109–6124 (2019). https://doi.org/10.1039/c9tb00897g
55. L.L. Hench, Bioceramics. J. Am. Ceram. Soc. **81**, 1705–1728 (1998)
56. A.F. Ali, Z.A. Alrowaili, E.M. El-Giar, M.M. Ahmed, A.M. El-Kady, Novel green synthesis of hydroxyapatite uniform nanorods via microwave-hydrothermal route using licorice root extract as template. Ceram. Int. **47**, 3928–3937 (2021). https://doi.org/10.1016/j.ceramint.2020.09.256
57. J. Indira, K.S. Malathi, Comparison of template mediated ultrasonic and microwave irradiation method on the synthesis of hydroxyapatite nanoparticles for biomedical applications. Mater. Today Proc. (2021). https://doi.org/10.1016/j.matpr.2021.03.028
58. J.S. Earl, D.J. Wood, S.J. Milne, Hydrothermal synthesis of hydroxyapatite. J. Phys. Conf. Ser. **26**, 268–271 (2006). https://doi.org/10.1088/1742-6596/26/1/064
59. D.M. Liu, T. Troczynski, W.J. Tseng, Water-based sol-gel synthesis of hydroxyapatite: process development. Biomaterials **22**, 1721–1730 (2001). https://doi.org/10.1016/S0142-9612(00)00332-X
60. S.H. Rhee, Synthesis of hydroxyapatite via mechanochemical treatment. Biomaterials **23**, 1147–1152 (2002). https://doi.org/10.1016/S0142-9612(01)00229-0
61. Y.J. Wang, C.J. Di, K. Wei, S.H. Zhang, X.D. Wang, Surfactant-assisted synthesis of hydroxyapatite particles. Mater. Lett. **60**, 3227–3231 (2006). https://doi.org/10.1016/j.matlet.2006.02.077
62. A. Yelten-Yilmaz, S. Yilmaz, Wet chemical precipitation synthesis of hydroxyapatite (HA) powders. Ceram. Int. **44**, 9703–9710 (2018). https://doi.org/10.1016/j.ceramint.2018.02.201
63. S.J. Lee, Y.S. Yoon, M.H. Lee, N.S. Oh, Nanosized hydroxyapatite powder synthesized from eggshell and phosphoric acid. J. Nanosci. Nanotechnol. **7**, 4061–4064 (2007). https://doi.org/10.1166/jnn.2007.067
64. A. Buekenhoudt, A. Kovalevsky, J. Luyten, F. Snijkers, in *1.11 - basic aspects in inorganic membrane preparation*, ed. by Drioli E, (Elsevier, Oxford, 2010), pp. 217–252. https://doi.org/10.1016/B978-0-08-093250-7.00011-6
65. S. Pramanik, A.K. Agarwal, K.N. Rai, A. Garg, Development of high strength hydroxyapatite by solid-state-sintering process. Ceram. Int. **33**, 419–426 (2007). https://doi.org/10.1016/j.ceramint.2005.10.025
66. M.H. Santos, M. de Oliveira, L.P.F. de Souza, H.S. Mansur, W.L. Vasconcelos, Synthesis control and characterization of hydroxyapatite prepared by wet precipitation process. Mater. Res. **7**, 625–630 (2004). https://doi.org/10.1590/s1516-14392004000400017

67. D. Moreno, F. Vargas, J. Ruiz, M.E. López, Solid-state synthesis of alpha tricalcium phosphate for cements used in biomedical applications. Bol. la Soc. Esp. Ceram. y Vidr. **59**, 193–200 (2020). https://doi.org/10.1016/j.bsecv.2019.11.004
68. K. Teshima, S.H. Lee, M. Sakurai, Y. Kameno, K. Yubuta, T. Suzuki, T. Shishido, M. Endo, S. Oishi, Well-formed one-dimensional hydroxyapatite crystals grown by an environmentally friendly flux method. Cryst. Growth Des. **9**, 2937–2940 (2009). https://doi.org/10.1021/cg900159j
69. H.R. Javadinejad, R. Ebrahimi-Kahrizsangi, Thermal and kinetic study of hydroxyapatite formation by solid-state reaction. Int. J. Chem. Kinet. **53**, 583–595 (2021). https://doi.org/10.1002/kin.21467
70. T. Rojac, M. Kosec, Mechanochemical synthesis of complex ceramic oxides. High-Energy Ball Milling (2010). https://doi.org/10.1533/9781845699444.2.113
71. R. Dorey, Routes to thick films. Ceram. Thick Film MEMS Microdevices (2012). https://doi.org/10.1016/b978-1-4377-7817-5.00002-x
72. F.C. Gennari, J.J. Andrade-Gamboa, A systematic approach to the synthesis, thermal stability and hydrogen storage properties of rare-earth borohydrides, *Emerging materials for energy conversion and storage* (Elsevier, Amsterdam, Netherlands, 2018), pp. 429–459. https://doi.org/10.1016/B978-0-12-813794-9.00013-2
73. N. Llorca-Isern, C. Artieda-Guzmán, Metal-based composite powders, *Advances in powder metallurgy: Properties, processing and applications* (Elsevier Inc, Sawston, Cambridge, United Kingdom, 2013), pp. 241–72. https://doi.org/10.1533/9780857098900.2.241
74. R.B. Schwarz, Introduction to the viewpoint set on: mechanical alloying. Scr. Mater. **34**, 1–4 (1996). https://doi.org/10.1016/1359-6462(95)00463-7
75. T.D. Shen, C.C. Koch, T.L. McCormick, R.J. Nemanich, J.Y. Huang, J.G. Huang, The structure and property characteristics of amorphous/nanocrystalline silicon produced by ball milling. J. Mater. Res. **10**, 139–148 (1995). https://doi.org/10.1557/JMR.1995.0139
76. K.C.B. Yeong, J. Wang, S.C. Ng, Mechanochemical synthesis of nanocrystalline hydroxyapatite from CaO and CaHPO4. Biomaterials **22**, 2705–2712 (2001). https://doi.org/10.1016/S0142-9612(00)00257-X
77. M.H. Fathi, E.M. Zahrani, Fabrication and characterization of fluoridated hydroxyapatite nanopowders via mechanical alloying. J. Alloys Compd. **475**, 408–414 (2009). https://doi.org/10.1016/j.jallcom.2008.07.058
78. T.K. Achar, A. Bose, P. Mal, Mechanochemical synthesis of small organic molecules. Beilstein J. Org. Chem. **13**, 1907–1931 (2017). https://doi.org/10.3762/bjoc.13.186
79. C. Shu, W. Yanwei, L. Hong, P. Zhengzheng, Y. Kangde, Synthesis of carbonated hydroxyapatite nanofibers by mechanochemical methods. Ceram. Int. **31**, 135–138 (2005). https://doi.org/10.1016/j.ceramint.2004.04.012
80. S. Dinda, A. Bhagavatam, H. Alrehaili, G.P. Dinda, Mechanochemical synthesis of nanocrystalline hydroxyapatite from $Ca(H_2PO_4)_2{\cdot}H_2O$, CaO, $Ca(OH)_2$, and P_2O_5 mixtures. Nanomaterials **10**, 1–10 (2020). https://doi.org/10.3390/nano10112232
81. S. Eiden-Aßmann, M. Viertelhaus, A. Heiß, K.A. Hoetzer, J. Felsche, The influence of amino acids on the biomineralization of hydroxyapatite in gelatin. J. Inorg. Biochem. **91**, 481–486 (2002). https://doi.org/10.1016/S0162-0134(02)00481-6
82. J. Zhan, Y.H. Tseng, J.C.C. Chan, C.Y. Mou, Biomimetic formation of hydroxyapatite nanorods by a single-crystal-to- single-crystal transformation. Adv. Funct. Mater. **15**, 2005–2010 (2005). https://doi.org/10.1002/adfm.200500274
83. D.W. Kim, I.S. Cho, J.Y. Kim, H.L. Jang, G.S. Han, H.S. Ryu, H. Shin, H.S. Jung, H. Kim, K.S. Hong, Simple large-scale synthesis of hydroxyapatite nanoparticles: In situ observation of crystallization process. Langmuir **26**, 384–388 (2010). https://doi.org/10.1021/la902157z
84. S. Catros, F. Guillemot, E. Lebraud, C. Chanseau, S. Perez, R. Bareille, J. Amédée, J.C. Fricain, Physico-chemical and biological properties of a nano-hydroxyapatite powder synthesized at room temperature. Irbm **31**, 226–233 (2010). https://doi.org/10.1016/j.irbm.2010.04.002
85. Y.H. Huang, Y.J. Shih, F.J. Cheng, Novel KMnO 4-modified iron oxide for effective arsenite removal. J. Hazard Mater. **198**, 1–6 (2011). https://doi.org/10.1016/j.jhazmat.2011.10.010
86. E. Bouyer, F. Gitzhofer, M.I. Boulos, Morphological study of hydroxyapatite nanocrystal suspension. J. Mater. Sci. Mater. Med. **11**, 523–531 (2000). https://doi.org/10.1023/A:1008918110156
87. A. Afshar, M. Ghorbani, N. Ehsani, M.R. Saeri, C.C. Sorrell, Some important factors in the wet precipitation process of hydroxyapatite. Mater. Des. **24**, 197–202 (2003). https://doi.org/10.1016/S0261-3069(03)00003-7
88. T. Matsumoto, K.I. Tamine, R. Kagawa, Y. Hamada, M. Okazaki, J. Takahashi, Different behavior of implanted hydroxyapatite depending on morphology, size and crystallinity. J. Ceram. Soc. Japan **114**, 760–762 (2006). https://doi.org/10.2109/jcersj.114.760
89. I. Mobasherpour, M.S. Heshajin, A. Kazemzadeh, M. Zakeri, Synthesis of nanocrystalline hydroxyapatite by using precipitation method. J. Alloys Compd. **430**, 330–333 (2007). https://doi.org/10.1016/j.jallcom.2006.05.018
90. G. Gecim, S. Dönmez, E. Erkoc, Calcium deficient hydroxyapatite by precipitation: continuous process by vortex reactor and semi-batch synthesis. Ceram. Int. **47**, 1917–1928 (2021). https://doi.org/10.1016/j.ceramint.2020.09.020
91. Y. Wang, X. Ren, X. Ma, W. Su, Y. Zhang, X. Sun, X. Li, Alginate-intervened hydrothermal synthesis of hydroxyapatite nanocrystals with nanopores. Cryst. Growth Des. **15**, 1949–1956 (2015). https://doi.org/10.1021/acs.cgd.5b00113
92. Y. Qi, J. Shen, Q. Jiang, B. Jin, J. Chen, X. Zhang, The morphology control of hydroxyapatite microsphere at high pH values by hydrothermal method. Adv. Powder Technol. **26**, 1041–1046 (2015). https://doi.org/10.1016/j.apt.2015.04.008
93. G. Zhang, J. Chen, S. Yang, Q. Yu, Z. Wang, Q. Zhang, Preparation of amino-acid-regulated hydroxyapatite particles by hydrothermal method. Mater. Lett. **65**, 572–574 (2011). https://doi.org/10.1016/j.matlet.2010.10.078
94. F. Nagata, Y. Yamauchi, M. Tomita, K. Kato, Hydrothermal synthesis of hydroxyapatite nanoparticles and their protein adsorption behavior. J. Ceram. Soc. Japan **121**, 797–801 (2013). https://doi.org/10.2109/jcersj2.121.797
95. N.A.S. Mohd Pu'ad, R.H. Abdul Haq, H. Mohd Noh, H.Z. Abdullah, M.I. Idris, T.C. Lee, Synthesis method of hydroxyapatite: a review. Mater. Today Proc. **29**, 233–239 (2019). https://doi.org/10.1016/j.matpr.2020.05.536
96. W.J. Shih, M.C. Wang, M.H. Hon, Morphology and crystallinity of the nanosized hydroxyapatite synthesized by hydrolysis using cetyltrimethylammonium bromide (CTAB) as a surfactant. J. Cryst. Growth **275**, 2339–2344 (2005). https://doi.org/10.1016/j.jcrysgro.2004.11.330
97. A. Almirall, G. Larrecq, J.A. Delgado, S. Martínez, J.A. Planell, M.P. Ginebra, Fabrication of low temperature macroporous hydroxyapatite scaffolds by foaming and hydrolysis of an α-TCP paste. Biomaterials **25**, 3671–3680 (2004). https://doi.org/10.1016/j.biomaterials.2003.10.066
98. M. Kavitha, R. Subramanian, K.S. Vinoth, R. Narayanan, G. Venkatesh, N. Esakkiraja, Optimization of process parameters

for solution combustion synthesis of strontium substituted hydroxyapatite nanocrystals using design of experiments approach. Powder Technol. **271**, 167–181 (2015). https://doi.org/10.1016/j.powtec.2014.10.046
99. J.S. Cho, J.C. Lee, S.H. Rhee, Effect of precursor concentration and spray pyrolysis temperature upon hydroxyapatite particle size and density. J. Biomed. Mater. Res. Part B Appl. Biomater. **104**, 422–430 (2016). https://doi.org/10.1002/jbm.b.33406
100. S. Sasikumar, R. Vijayaraghavan, Synthesis and characterization of bioceramic calcium phosphates by rapid combustion synthesis. J. Mater. Sci. Technol. **26**, 1114–1118 (2010). https://doi.org/10.1016/S1005-0302(11)60010-8
101. R. Ayers, N. Hannigan, N. Vollmer, C. Unuvar, Combustion synthesis of heterogeneous calcium phosphate bioceramics from calcium oxide and phosphate precursors. Int. J. Self Propag. High Temp. Synth. **20**, 6–14 (2011). https://doi.org/10.3103/S1061386211010031
102. R. Ramakrishnan, P. Wilson, T. Sivakumar, I. Jemina, A comparative study of hydroxyapatites synthesized using various fuels through aqueous and alcohol mediated combustion routes. Ceram. Int. **39**, 3519–3532 (2013). https://doi.org/10.1016/j.ceramint.2012.10.176
103. N. Wakiya, M. Yamasaki, T. Adachi, A. Inukai, N. Sakamoto, D. Fu, O. Sakurai, K. Shinozaki, H. Suzuki, Preparation of hydroxyapatite-ferrite composite particles by ultrasonic spray pyrolysis. Mater. Sci. Eng. B Solid State Mater. Adv. Technol. **173**, 195–198 (2010). https://doi.org/10.1016/j.mseb.2009.12.013
104. W. Widiyastuti, A. Setiawan, S. Winardi, T. Nurtono, H. Setyawan, Particle formation of hydroxyapatite precursor containing two components in a spray pyrolysis process. Front. Chem. Sci. Eng. **8**, 104–113 (2014). https://doi.org/10.1007/s11705-014-1406-1
105. G.H. An, H.J. Wang, B.H. Kim, Y.G. Jeong, Y.H. Choa, Fabrication and characterization of a hydroxyapatite nanopowder by ultrasonic spray pyrolysis with salt-assisted decomposition. Mater. Sci. Eng. A **449–451**, 821–824 (2007). https://doi.org/10.1016/j.msea.2006.02.436
106. J.S. Cho, Y.C. Kang, Nano-sized hydroxyapatite powders prepared by flame spray pyrolysis. J. Alloys Compd. **464**, 282–287 (2008). https://doi.org/10.1016/j.jallcom.2007.09.092
107. M.E. Zilm, L. Chen, V. Sharma, A. McDannald, M. Jain, R. Ramprasad, M. Wei, Hydroxyapatite substituted by transition metals: experiment and theory. Phys. Chem. Chem. Phys. **18**, 16457–16465 (2016). https://doi.org/10.1039/c6cp00474a
108. M. Frasnelli, F. Cristofaro, V.M. Sglavo, S. Dirè, E. Callone, R. Ceccato, G. Bruni, A.I. Cornaglia, L. Visai, Synthesis and characterization of strontium-substituted hydroxyapatite nanoparticles for bone regeneration. Mater. Sci. Eng. C **71**, 653–662 (2017). https://doi.org/10.1016/j.msec.2016.10.047
109. S.Y. Park, K.-I. Kim, S.P. Park, J.H. Lee, H.S. Jung, Aspartic acid-assisted synthesis of multifunctional strontium-substituted hydroxyapatite microspheres. Cryst. Growth Des. **16**, 4318–4326 (2016). https://doi.org/10.1021/acs.cgd.6b00420
110. J. Li, L. Yang, X. Guo, W. Cui, S. Yang, J. Wang, Y. Qu, Z. Shao, S. Xu, Osteogenesis effects of strontium-substituted hydroxyapatite coatings on true bone ceramic surfaces in vitro and in vivo. Biomed. Mater. (2018). https://doi.org/10.1088/1748-605X/aa89af
111. J. Li, X. Liu, S. Park, A.L. Miller, A. Terzic, L. Lu, Strontium-substituted hydroxyapatite stimulates osteogenesis on poly(propylene fumarate) nanocomposite scaffolds. J. Biomed. Mater. Res. Part A **107**, 631–642 (2019). https://doi.org/10.1002/jbm.a.36579
112. Z. Geng, X. Wang, J. Zhao, Z. Li, L. Ma, S. Zhu, Y. Liang, Z. Cui, H. He, X. Yang, The synergistic effect of strontium-substituted hydroxyapatite and microRNA-21 on improving bone remodeling and osseointegration. Biomater. Sci. **6**, 2694–2703 (2018). https://doi.org/10.1039/c8bm00716k
113. F. Tamimi, N.D. Le, D.C. Bassett, S. Ibasco, U. Gbureck, J. Knowles, A. Wright, A. Flynn, S.V. Komarova, J.E. Barralet, Biocompatibility of magnesium phosphate minerals and their stability under physiological conditions. Acta Biomater. **7**, 2678–2685 (2011). https://doi.org/10.1016/j.actbio.2011.02.007
114. A. Ewald, K. Helmschrott, G. Knebl, N. Mehrban, L.M. Grover, U. Gbureck, Effect of cold-setting calcium- and magnesium phosphate matrices on protein expression in osteoblastic cells. J Biomed Mater Res Part B Appl Biomater **96 B**, 326–332 (2011). https://doi.org/10.1002/jbm.b.31771
115. N.C. Andrés, N.L. D'Elía, J.M. Ruso, A.E. Campelo, V.L. Massheimer, P.V. Messina, Manipulation of Mg^{2+}-Ca^{2+} switch on the development of bone mimetic hydroxyapatite. ACS Appl. Mater. Interfaces **9**, 15698–15710 (2017). https://doi.org/10.1021/acsami.7b02241
116. I. Uysal, F. Severcan, A. Tezcaner, Z. Evis, Co-doping of hydroxyapatite with zinc and fluoride improves mechanical and biological properties of hydroxyapatite. Prog. Nat. Sci. Mater. Int. **24**, 340–349 (2014). https://doi.org/10.1016/j.pnsc.2014.06.004
117. M. Irfan, S.N. Sultana, B. Venkateswarlu, M. Jagannatham, R. Dumpala, B.R. Sunil, Zinc-substituted hydroxyapatite: synthesis, structural analysis, and antimicrobial behavior. Trans. Indian Inst. Met. **74**, 2335–2344 (2021). https://doi.org/10.1007/s12666-021-02290-x
118. E.S. Thian, J. Huang, S.M. Best, Z.H. Barber, W. Bonfield, Silicon-substituted hydroxyapatite: the next generation of bioactive coatings. Mater. Sci. Eng. C **27**, 251–256 (2007). https://doi.org/10.1016/j.msec.2006.05.016
119. Y.O. Nikitina, N.V. Petrakova, A.A. Ashmarin, D.D. Titov, S.V. Shevtsov, T.N. Penkina, E.A. Kuvshinova, S.M. Barinov, V.S. Komlev, N.S. Sergeeva, Preparation and properties of copper-substituted hydroxyapatite powders and ceramics. Inorg. Mater. **55**, 1061–1067 (2019). https://doi.org/10.1134/S002016851910011X
120. A. Elrayah, W. Zhi, S. Feng, S. Al-Ezzi, H. Lei, J. Weng, Preparation of micro/nano-structure copper-substituted hydroxyapatite scaffolds with improved angiogenesis capacity for bone regeneration. Materials (Basel) (2018). https://doi.org/10.3390/ma11091516
121. J. Sang Cho, S.H. Um, D. Su Yoo, Y.C. Chung, S. Hye Chung, J.C. Lee, S.H. Rhee, Enhanced osteoconductivity of sodium-substituted hydroxyapatite by system instability. J. Biomed. Mater. Res. Part B Appl. Biomater. **102**, 1046–1062 (2014). https://doi.org/10.1002/jbm.b.33087
122. W.E. Cabrera, I. Schrooten, M.E. De Broe, P.C. D'Haese, Strontium and bone. J. Bone Miner. Res. **14**, 661–668 (1999). https://doi.org/10.1359/jbmr.1999.14.5.661
123. C. Li, O. Paris, S. Siegel, P. Roschger, E.P. Paschalis, K. Klaushofer, P. Fratzl, Strontium is incorporated into mineral crystals only in newly formed bone during strontium ranelate treatment. J. Bone Miner. Res. **25**, 968–975 (2010). https://doi.org/10.1359/jbmr.091038
124. G. Boivin, D. Farlay, M.T. Khebbab, X. Jaurand, P.D. Delmas, P.J. Meunier, In osteoporotic women treated with strontium ranelate, strontium is located in bone formed during treatment with a maintained degree of mineralization. Osteoporos. Int. **21**, 667–677 (2010). https://doi.org/10.1007/s00198-009-1005-z
125. P. Roschger, I. Manjubala, N. Zoeger, F. Meirer, R. Simon, C. Li, N. Fratzl-Zelman, B.M. Misof, E.P. Paschalis, C. Streli, P. Fratzl, K. Klaushofer, Bone material quality in transiliac bone biopsies of postmenopausal osteoporotic women after 3 years of

strontium ranelate treatment. J. Bone Miner. Res. **25**, 891–900 (2010). https://doi.org/10.1359/jbmr.091028
126. J. Christoffersen, M.R. Christoffersen, N. Kolthoff, O. Bärenholdt, Effects of strontium ions on growth and dissolution of hydroxyapatite and on bone mineral detection. Bone **20**, 47–54 (1997). https://doi.org/10.1016/S8756-3282(96)00316-X
127. H. Zhu, D. Guo, L. Sun, H. Li, D.A.H. Hanaor, F. Schmidt, K. Xu, Nanostructural insights into the dissolution behavior of Sr-doped hydroxyapatite. J. Eur. Ceram. Soc. **38**, 5554–5562 (2018). https://doi.org/10.1016/j.jeurceramsoc.2018.07.056
128. K. Zhu, K. Yanagisawa, R. Shimanouchi, A. Onda, K. Kajiyoshi, Preferential occupancy of metal ions in the hydroxyapatite solid solutions synthesized by hydrothermal method. J. Eur. Ceram. Soc. **26**, 509–513 (2006). https://doi.org/10.1016/j.jeurceramsoc.2005.07.019
129. K. Kandori, M. Saito, H. Saito, A. Yasukawa, T. Ishikawa, Adsorption of protein on non-stoichiometric calcium-strontium hydroxyapatite. Colloids Surf. A Physicochem. Eng. Asp. **94**, 225–230 (1995). https://doi.org/10.1016/0927-7757(94)02969-5
130. E. Landi, G. Logroscino, L. Proietti, A. Tampieri, M. Sandri, S. Sprio, Biomimetic Mg-substituted hydroxyapatite: From synthesis to in vivo behaviour. J. Mater. Sci. Mater. Med. **19**, 239–247 (2008). https://doi.org/10.1007/s10856-006-0032-y
131. S. Gomes, G. Renaudin, E. Jallot, J.M. Nedelec, Structural characterization and biological fluid interaction of sol-gel-derived Mg-substituted biphasic calcium phosphate ceramics. ACS Appl. Mater. Interfaces **1**, 505–513 (2009). https://doi.org/10.1021/am800162a
132. E. Landi, A. Tampieri, M. Mattioli-Belmonte, G. Celotti, M. Sandri, A. Gigante, P. Fava, G. Biagini, Biomimetic Mg- and Mg, CO3-substituted hydroxyapatites: synthesis characterization and in vitro behaviour. J. Eur. Ceram. Soc. **26**, 2593–2601 (2006). https://doi.org/10.1016/j.jeurceramsoc.2005.06.040
133. S. Lala, M. Ghosh, P.K. Das, D. Das, T. Kar, S.K. Pradhan, Magnesium substitution in carbonated hydroxyapatite: structural and microstructural characterization by Rietveld's refinement. Mater. Chem. Phys. **170**, 319–329 (2016). https://doi.org/10.1016/j.matchemphys.2015.12.058
134. A.A. Chaudhry, J. Goodall, M. Vickers, J.K. Cockcroft, I. Rehman, J.C. Knowles, J.A. Darr, Synthesis and characterisation of magnesium substituted calcium phosphate bioceramic nanoparticles made via continuous hydrothermal flow synthesis. J. Mater. Chem. **18**, 5900–5908 (2008). https://doi.org/10.1039/b807920j
135. A. Farzadi, F. Bakhshi, M. Solati-Hashjin, M. Asadi-Eydivand, N.A.A. Osman, Magnesium incorporated hydroxyapatite: synthesis and structural properties characterization. Ceram. Int. **40**, 6021–6029 (2014). https://doi.org/10.1016/j.ceramint.2013.11.051
136. J.P. O'Connor, D. Kanjilal, M. Teitelbaum, S.S. Lin, J.A. Cottrell, Zinc as a therapeutic agent in bone regeneration. Materials (Basel) **13**, 1–22 (2020). https://doi.org/10.3390/ma13102211
137. M. Yamaguchi, R. Yamaguchi, Action of zinc on bone metabolism in rats. Increases in alkaline phosphatase activity and DNA content. Biochem. Pharmacol. **35**, 773–777 (1986). https://doi.org/10.1016/0006-2952(86)90245-5
138. C. Ergun, T.J. Webster, R. Bizios, R.H. Doremus, Hydroxylapatite with substituted magnesium, zinc, cadmium, and yttrium. I. Structure and microstructure. J. Biomed. Mater. Res. **59**, 305–311 (2002). https://doi.org/10.1002/jbm.1246
139. F. Miyaji, Y. Kono, Y. Suyama, Formation and structure of zinc-substituted calcium hydroxyapatite. Mater. Res. Bull. **40**, 209–220 (2005). https://doi.org/10.1016/j.materresbull.2004.10.020
140. M. Li, X. Xiao, R. Liu, C. Chen, L. Huang, Structural characterization of zinc-substituted hydroxyapatite prepared by hydrothermal method. J. Mater. Sci. Mater. Med. **19**, 797–803 (2008). https://doi.org/10.1007/s10856-007-3213-4
141. Z. Zhong, J. Qin, J. Ma, Rapid synthesis of citrate-zinc substituted hydroxyapatite using the ultrasonication-microwave method. Ceram. Int. **43**, 13308–13313 (2017). https://doi.org/10.1016/j.ceramint.2017.07.029
142. E.S. Thian, T. Konishi, Y. Kawanobe, P.N. Lim, C. Choong, B. Ho, M. Aizawa, Zinc-substituted hydroxyapatite: a biomaterial with enhanced bioactivity and antibacterial properties. J. Mater. Sci. Mater. Med. **24**, 437–445 (2013). https://doi.org/10.1007/s10856-012-4817-x
143. E.M. Carlisle, Silicon: a requirement in bone formation independent of vitamin D1. Calcif. Tissue Int. **33**, 27–34 (1981). https://doi.org/10.1007/BF02409409
144. W. Götz, E. Tobiasch, S. Witzleben, M. Schulze, Effects of silicon compounds on biomineralization, osteogenesis, and hard tissue formation. Pharmaceutics **11**, 1–27 (2019). https://doi.org/10.3390/pharmaceutics11030117
145. E.M. Carlisle, Silicon: a possible factor in bone calcification. Science **167**(3916), 279–280 (1970). https://doi.org/10.1126/science.167.3916.279
146. L.T. Bang, B.D. Long, R. Othman, Carbonate hydroxyapatite and silicon-substituted carbonate hydroxyapatite: synthesis, mechanical properties, and solubility evaluations. Sci. World J. (2014). https://doi.org/10.1155/2014/969876
147. A. Tsalsabila, Y.W. Sari, A. Maddu, Synthesis of silicon substituted hydroxyapatite using microwave irradiation, in: Proc—2018 1st Int Conf Bioinformatics, Biotechnol Biomed Eng BioMIC 2018, vol. 1, pp. 1–5 (2019). https://doi.org/10.1109/BIOMIC.2018.8610598
148. C. Palacios, The role of nutrients in bone health, from A to Z. Crit. Rev. Food Sci. Nutr. **46**, 621–628 (2006). https://doi.org/10.1080/10408390500466174
149. S. Shanmugam, B. Gopal, Copper substituted hydroxyapatite and fluorapatite: synthesis, characterization and antimicrobial properties. Ceram. Int. **40**, 15655–15662 (2014). https://doi.org/10.1016/j.ceramint.2014.07.086
150. H.J. Kronzucker, D. Coskun, L.M. Schulze, J.R. Wong, D.T. Britto, Sodium as nutrient and toxicant. Plant Soil **369**, 1–23 (2013). https://doi.org/10.1007/s11104-013-1801-2
151. R. Mangili, J.J. Bending, G. Scott, L.K. Li, A. Gupta, G. Viberti, Increased sodium-lithium countertransport activity in red cells of patients with insulin-dependent diabetes and nephropathy. N. Engl. J. Med. **318**, 146–150 (1988)
152. K. Hu, B.R. Olsen, The roles of vascular endothelial growth factor in bone repair and regeneration. Bone **91**, 30–38 (2016). https://doi.org/10.1016/j.bone.2016.06.013